UNIVERSITEIT VAN PRETORIA
UNIVERSITY OF PRETORIA
YUNIBESITHI YA PRETORIA

THE EFFECT OF ADJACENT TUBES ON THE DIABATIC FRICTION FACTORS IN THE TRANSITIONAL FLOW REGIME

BY: F. A. MULOCK-HOUWER

SUBMITTED IN PARTIAL FULFILMENT OF THE REQUIREMENTS FOR THE DEGREE:
MASTER OF ENGINEERING

DEPARTMENT OF MECHANICAL AND AERONAUTICAL ENGINEERING.

UNIVERSITY OF PRETORIA

YEAR: 2015

SUPERVISOR: PROF J. P. MEYER

ABSTRACT

Title: The effect of adjacent tubes on the diabatic friction factors in the transitional flow regime

Supervisor: Professor J. P. Meyer

Department: Mechanical and Aeronautical Engineering

Degree: Master of Engineering (Mechanical Engineering)

Heat exchangers are used throughout the world in important processes such as the generation of electrical energy. Modern heat exchangers are often forced to operate in the transitional flow regime, where flow can be unpredictable. Most of the research that has been done on the transitional flow regime has focussed on the influence of heat transfer and the inlet effects. However, all these studies made use of only a single tube, while most heat exchangers would typically have a bundle of tubes such as in shell-and-tube type heat exchangers. The purpose of this study was to investigate the effect of adjacent tubes on the transitional flow regime during diabatic conditions. An experimental set-up was purposefully built for this investigation and two test sections were investigated. A single-tube test section was built for validation purposes, since similar work has been done. A triple-tube test section was built with three tubes spaced at a pitch distance of 1.4 outer diameters. The mass flow rate, as well as the pressure drops over the fully-developed section was measured for each tube. From the pressure drop data the friction factors were calculated. Furthermore, a heat flux of 3 kW/m^2 was applied to each tube and the inlet, outlet and wall temperatures were measured, to ensure that specifically the diabatic friction factors were determined. Water was used as the working fluid and tests were run over a Reynolds number range of 1 000 - 6 500. An uncertainty analysis showed the maximum uncertainty of the friction factors to be 8.3%. The laminar, transitional and turbulent flow regimes could be identified from the friction factor data. The results from the single-tube test section correlated well to the literature with transition starting at a Reynolds number of 2 380 and ending at 3 050. The results from the triple-tube test section showed the start of transition to be initiated by the presence of adjacent tubes, with the Centre-tube entering transition at a Reynolds number of 1 970. The outer tubes experience a delayed start in transition at Reynolds numbers of 3 000 and 2 800 for the Left-tube and Right-tube respectively. The end of transition occurred at approximately the same Reynolds number (3 100) for all three tubes of the triple-tube test section. Since the Centre-tube entered transition earlier than the outer tubes, maldistribution was evident, with the water taking the path of least resistance. The flow rate in the Centre-tube showed an average difference of 2.8% in the Reynolds number range of 1 970 to 3 150. Maldistribution proved to be negligible when all three tubes were in the laminar or turbulent flow regimes.

ACKNOWLEDGEMENTS:

- Professor J. P. Meyer, for his support and guidance throughout the study.
- Danie Gouws, for his vast experience throughout the building of the experimental set-up and test periods.
- The N. R. F. and D. S. T., for their financial support.
- Marilize Everts, for her support and encouragement throughout the study.
- Andrew Hall and Erin Vause, for their support in the building of the experimental set-up.

TABLE OF CONTENTS

LIST OF FIGURES:

LIST OF TABLES

LIST OF SYMBOLS

Symbol:	Description:	Units:
English		
A_s	Surface area	[m²]
d	Inner diameter of tube	[m]
D	Mass diffusivity	[m²/s]
C_p	Constant pressure specific heat	[J/kgK]
C_f	Friction coefficient	[-]
f	Darcy-Weisbach friction factor	[-]
Gr	Grashoff number	[-]
h	Heat transfer coefficient	[W/m²K]
I	Electric current	[A]
j	Colburn J-factor	[-]
k	Thermal conductivity of fluid	[W/mK]
L	Tube length	[m]
$\dot{m}$	Mass flow rate	[kg/s]
Nu	Nusselt number	[-]
Pr	Prandtl number	[-]
Δp	Differential pressure drop	[Pa]
$\dot{Q}$	Heat transfer rate	[W]
$\dot{q}$	Heat flux	[W/m²]
Re	Reynolds number	[-]
St	Stanton number	[-]
T	Temperature	[°C]
V	Average fluid velocity in tube	[m/s]
$\dot{V}$	Volume flow rate	[m³/s]
V	Electrical potential	[V]
x	Distance along the test section from the inlet	[m]
Greek		
β	Thermal expansion coefficient	[K⁻¹]
μ	Dynamic viscosity of fluid	[kg/ms]
η	Maldistribution velocity ratio	[-]
ν	Kinematic viscosity	[m²/s]
ρ	Density	[kg/m³]
τ	Shear stress	[Pa]
ε	Electrical resistivity	[Ωm]
Subscripts		
avg	Average value	
b	Bulk fluid	
i	Inlet or inner	
c	Centre between two pressure taps (Figure 3.6)	
cs	Cross-section	
cr	Critical	
e	Exit or outlet	
o	Outer	
s	Surface	
T	Thermal	
w	Wall	
∞	Surrounding air/environment	

1. INTRODUCTION

1.1. BACKGROUND

Energy generation is one of the biggest challenges faced by modern engineers. As technology becomes ever more accessible to the average person, the need for reliable and efficient ways of electrical energy generation constantly increases. With a world population that is ever growing it is clear that energy generation is not only a challenge now, but will be for the foreseeable future. Although many methods of electricity generation exist, most of them involve the heating, cooling or flow of a working fluid [1]. Heat exchangers are devices used to transfer thermal energy from one substance to another and form a vital part in the generation of electricity for our world population. The design of these heat exchangers is of utmost importance, since they have a direct impact on the efficiency of electricity generation.

Heat exchangers are not unique to the energy generation industry, but are also essential to thousands of other processes that affect our lives on a daily basis. Heat exchangers are used in almost every process where heating or cooling of a fluid or gas is needed. Air-conditioning systems, car radiators and fridges are a few examples where heat exchangers are part of daily human life [2].

Although heat exchangers come in many different forms and shapes, they are all designed to achieve one goal, which is to transfer heat from a fluid at a higher temperature to a fluid at a lower temperature [3]. Heat transfer can occur in three modes, conduction, convection and radiation. However, in most heat exchangers the dominant form of heat transfer is through convection and thus the other modes are usually labelled negligible. The movement of the fluid through the heat exchanger affects the rate at which convection heat transfer can occur, which proves to show that heat transfer and flow go hand in hand, especially when it comes to the design of heat exchangers.

Shell-and-tube heat exchangers, the most common type of heat exchanger in industry, are prone to operate in or near the transitional flow regime due to pumping considerations [4]. The tube-side of these heat exchangers sees a fluid entering through a single inlet before the flow is distributed to multiple tubes through an inlet header. The heat transfer coefficient on the tube-side is of great importance to the design of these heat exchangers since the tube-side usually has a much lower heat transfer coefficient than the shell side.

Most of the research done on the tube-side of shell-and-tube heat exchangers focussed on reducing flow maldistribution. Maldistribution refers to a non-uniform distribution of the fluid to the multiple tubes. It presents a problem for heat exchanger designers, as one of the first assumptions made in the design process is that the flow is separated uniformly to all the tubes. Studies have shown maldistribution to be affected by multiple parameters such as the pressure drop through the tubes, as well as the design of the inlet header.

A paper published by Kim *et al*. [5] tested four different inlet header designs. They showed that by a simple change in the position of the inlet tube the extent of maldistribution can be reduced greatly with only a small increase in pressure drop. Studies by Lalot *et al.* [6] and Wang *et al*. [7] proved that a porous baffle insert into the inlet header can also help improve the flow uniformity without a significant increase in header size. They also showed that reverse flow is a possibility in the outer tubes of a shell-and-tube heat exchanger if the inlet header has been poorly designed. Reverse flow could have a negative effect on the efficiency of the heat exchanger and should be avoided at all costs.

1.2. STATE OF THE ART OF THE TRANSITIONAL FLOW REGIME

The state of the art for the transitional flow regime was summarised in a keynote paper by Meyer [4] of the University of Pretoria. It follows from the paper that most of the research into the transitional flow regime has been done by Ghajar from Oklahoma State University, Meyer from the University of Pretoria and their relative co-workers.

Ghajar and co-workers investigated the effect of inlet geometry and heating on the transitional flow regime [8-10]. They focussed mostly on fully developed flow through smooth tubes using a constant heat flux boundary condition.

Their adiabatic and diabatic results showed that inlet geometry significantly affects the start and end of transition. The results showed that smoother inlet geometries, such as a bell-mouth, tended to delay the start of transition while rougher inlets, such as a re-entrant inlet tended to aggravate transition.

When heat transfer was present, they found that the start of transition was influenced more than the end of transition. This was caused by the effect of secondary flow, which is more profound at lower flow rates. Their results showed that an increase in heat flux delayed transition.

Meyer and co-workers also investigated the effect of inlet geometry and heating on the transitional flow regime inside circular tubes [11-14]. However, they made use of a constant surface temperature boundary condition and used water as the working fluid, where Ghajar made use of a water glycol mixture with a much higher Prandtl number.

Meyer and co-workers had similar findings to the work of Ghajar. The adiabatic results showed that smoother inlets tend to delay transition while rougher inlets showed an earlier start to transition. However, the results in this case showed that transition is not affected by inlet geometry when heat transfer was investigated. This result was in contrast to the work by Ghajar, but was attributed to the difference in Prandtl number of the two experiments.

Meyer and Olivier also investigated enhanced tubes and their heat transfer characteristics in the laminar, transition and turbulent flow regimes [11, 12]. This investigation was similar to the smooth tube tests in the sense that different inlets were used under diabatic and adiabatic conditions.

The heat transfer results showed that enhanced tubes reach significantly higher heat transfer coefficients in the turbulent flow regime, when compared to standard tubes. However, the results showed that in the laminar flow regime, standard tubes would tend to out preform enhanced tubes. They found that the helical fins inside enhanced tubes tend to obstruct secondary flow at low Reynolds numbers, thus neutralising any gain in heat transfer coefficient due to secondary flow. Their results also showed that enhanced tubes tend to aggravate transition, with transition starting and ending at significantly lower Reynolds numbers when compared to smooth tubes.

A nanofluid study done by Meyer *et al.* [15] investigated pressure drop characteristics for a smooth circular tube in the transitional flow regime. Aqueous suspensions of multi-walled carbon nanotubes at varying concentrations were used as the working fluid. Their results showed that the concentration of the carbon nanotubes significantly decreased the friction factors in the laminar flow regime. In the turbulent flow regime, the effect of the nanofluid concentration was similar but less prominent.

An investigation into heat transfer and pressure drop in rectangular micro-channels was conducted by Dirker *et al.* [16]. Three inlet configurations were investigated, namely, bell-mouth, swirl and sudden-contraction. Their results showed that the bell-mouth and swirl inlets

yielded significant heat transfer increases and minor friction factor increases when compared to the sudden-contraction inlet. The results also showed the swirl inlet to enter transition the earliest, followed by the bell-mouth and the sudden contraction inlets respectively.

More recent work done by Everts [17] investigated developing flow. Her findings were similar to the studies investigating fully-developed flow, with an increase in heat flux delaying the start of transition.

1.3. PROBLEM STATEMENT

Most of the previous research into the transitional flow regime has focussed on only a single tube and the inlet conditions to the tube. However, in modern heat exchangers a bundle of tubes are connected to an inlet header. Some research has been done on the optimisation of these inlet headers with the aim of improving the flow distribution through the multiple tubes, however, the effect of the tube spacing itself has not been investigated. Design guides specify a minimum pitch distance of 1.25 times the outer diameter of the tubes, based on the space required for cleaning the outer surface of the tubes. Most design guides only consider the effect of the tube pitch on the flow around the tube bundle, even though the flow inside the tubes tends to control the overall efficiency of the heat exchanger.

1.4. JUSTIFICATION

Shell-and-tube heat exchangers are normally designed to operate in the turbulent flow regime. However, Meyer [4] pointed out that cases occur where these types of heat exchangers might operate in or close to the transitional flow regime for the following reasons:

- In countries with extremely cold climates, water is often substituted for water-glycol mixtures as the working fluid. This fluid has a much higher Prandtl number and thus a much higher viscosity than water, which presents a challenge in terms of required pumping power and operating pressure. Therefore, these heat exchangers usually operate at lowered mass flow rates, where the resulting flow conditions are close to or in the transition region.
- Flow maldistribution refers to the case in which the flow is imperfectly distributed to the multiple tubes of a shell-and-tube heat exchanger. The resulting flow conditions might be that some tubes operate in or close to the transitional flow regime.
- Corrosion and scale build up inside the tubes cause the pressure drop to increase correspondingly. This increased flow resistance causes a decrease in mass flow rate which would shift the flow conditions closer to the transition region.

Furthermore, Lalot *et al.* [6] showed that poorly designed inlet headers of shell-and-tube heat exchangers could lead to reverse flow in some of the tubes.

Since literature (discussed in Section 1.2) showed that the inlet geometry to a tube has a significant effect on the flow conditions in the transitional flow regime, it would be reasonable to suspect that adjacent tubes, as in the tube bundle of a shell-and-tube heat exchanger, cause an inlet effect. These inlet effects would influence the resulting pressure drop characteristics.

1.5. AIM OF THE STUDY

The purpose of this study was to determine the effect of adjacent tubes on the diabatic friction factor in the transitional flow regime. The study was limited to three tubes only.

1.6. OBJECTIVES OF THE STUDY

The objectives of this study were:

- To design and build an experimental set-up capable of doing highly accurate pressure drop and heat transfer measurements on a single-tube and a triple-tube test section.

- To validate the experimental set-up and measurements against previous experimental investigations using the single-tube test section.
- To obtain the average friction factor data across each tube length over a wide range of Reynolds numbers for the triple-tube test section.
- To investigate the effect of the adjacent tubes on the start and end of transition.

1.7. SCOPE OF WORK

This study was the outcome of a nine month research masters, with report writing and examination in the three months thereafter. The biggest part of the project was the design, build and commissioning of the experimental set-up, since it needed to be built from scratch by the author and two fellow researchers. The process included sizing, specifying and ordering equipment; building the plant and test sections; as well as testing and troubleshooting before commissioning the entire experimental set-up. Eight months were spent on the experimental set-up, which left only one month for testing.

To simulate the effect of adjacent tubes, three smooth tubes were tested in a horizontal layout with a tube pitch distance of 1.4 times the outer tube diameter, or 8.4 mm. Due to financial and time constraints the study was limited to a single tube pitch and a single heat flux. However, the plant was designed and built to accommodate future work into different tube pitches, tube layouts and heat fluxes.

1.8. OVERVIEW OF DISSERTATION

This report is aimed at presenting pressure drop data for a single-tube and a triple-tube test section operating in the transitional flow regime.

Chapter 2 contains an in depth literature review, focussing on previous investigations into the transitional flow regime, as well as some work done on maldistribution in tube bundles. Chapter 3 contains details of the experimental set-up, test sections, testing methodology and the uncertainty analysis. Chapter 4 contains the details of the validation process where the data from the single-tube test section was compared to the results from previous studies. Chapter 5 presents and discusses the results of the investigation into the triple-tube test section. Chapter 6 serves as the summary and conclusion of the dissertation where logical deductions where drawn and recommendations were made for future work.

2. LITERATURE REVIEW

2.1. INTRODUCTION

In this chapter some background information is given on terminology and parameters used in this study. Furthermore, a summary is given of all the work that has been done on the transitional flow for horizontal circular tubes that relates to this study. The leading researchers on this topic are Professor Afshin Ghajar from Oklahoma State University and Professor Josua Meyer from the University of Pretoria; their work is summarised and compared in Section 2.3. Lastly, Section 2.3 contains a summary of studies into flow maldistribution through horizontal circular tubes.

2.2. BACKGROUND AND NON-DIMENSIONAL PARAMETERS

2.2.1. REYNOLDS NUMBER

The Reynolds number, named after Osborne Reynolds, is a dimensionless coefficient often used when studying forced convection to categorise flow into the laminar, transitional or turbulent regime. According to White [18] the Reynolds number can be seen as a parameter that correlates the viscous behaviour of all Newtonian fluids. For flow in a circular tube, the Reynolds number can be calculated using Equation 2.1:

$$Re_d = \frac{\rho V d}{\mu} \qquad [2.1]$$

Equation 2.1 shows that the average velocity of the fluid will determine the Reynolds number when the tube diameter, density and dynamic viscosity are kept constant. At relatively low velocities fluid flow is orderly and directional, this is known as laminar flow regime. At higher Reynolds numbers (high flow velocity) the fluid seems chaotic and this is categorised as the turbulent flow regime. However, it has been documented that flow conditions cannot go from laminar directly to turbulent; the region in between sees the flow behaving orderly at times and chaotic at times and is called the transition region or the transitional flow regime.

2.2.2. FRICTION FACTOR

The Darcy friction factor, also known as the Moody friction factor is a dimensionless variable used in the Darcy–Weisbach equation and relates to the wall shear stress of the fluid as shown in in Equation 2.2.

$$f = \frac{\pi^2 \tau_w \rho \, d^4}{2 \, \dot{m}^2} \qquad [2.2]$$

The friction factor is an important dimensionless parameter as it gives a measure of the frictional losses and thus relates directly to the pressure drop through tubes. When considering tube flow the pressure drop is always an important factor since it relates directly to pumping power. The Darcy–Weisbach equation for flow through circular tubes can be seen in Equation 2.3.

$$f = \frac{\Delta p \, \rho \, d^5 \pi^2}{8 \, \dot{m}^2 L} \qquad [2.3]$$

For single-phase fully-developed through circular tubes, the laminar friction factors can be predicted by the Poiseuille [19] equation:

$$f_{lam} = \frac{64}{Re} \qquad [2.4]$$

For turbulent flow conditions the Blasius [20] and Filonenko [21] equations are commonly used and are presented in Equations 2.5 and 2.6 respectively.

$$f_{turb} = 0.316Re^{-0.25} \qquad (Re \leq 2 \times 10^4) \quad [2.5]$$

$$f_{turb} = (0.79 \ln Re - 1.64)^{-2} \quad (2 \times 10^4 \leq Re \leq 2 \times 10^6) \quad [2.6]$$

Fang *et al.* [21] suggested the Reynolds number ranges of Equations 2.5 and 2.6 to remain relatively accurate. Much later Danish *et al.* [22] proposed a correlation that would predict the friction factors for both the laminar and turbulent flow regimes:

$$\frac{1}{2\sqrt{f}} = A - \frac{1.73718A \ln A}{1.73718+A} + \frac{2.62122A(\ln A)^2}{(1.73718+A)^3} + \frac{3.03568A(\ln A)^3}{(1.73718+A)^4} \quad [2.7a]$$

$$A = 4 \log Re - 0.4 \quad [2.7b]$$

Allen and Eckert [23] proposed a modified version of the Blasius equation that accounts for the difference in viscosity between the tube wall and the centre of the tube due to the temperature gradient:

$$f_{turb} = 0.316Re^{-0.25}\left(\frac{\mu_b}{\mu_w}\right)^{-0.25} \quad [2.8]$$

However, the viscosity ratio tends to stay close to unity unless very high heat fluxes are applied to the tube. Thus the standard Blasius equation is seen as sufficient for most friction factor predictions in the turbulent flow regime.

2.2.3. NATURAL CONVECTION AND THE INFLUENCE OF SECONDARY FLOW

Heat transfer can be classified into three main modes: conduction, radiation and convection [2]. Heat transfer can only occur via convection if there is movement of the respective fluid (liquid or gas). However, the movement of the fluid can be induced in two different ways:

Forced convection requires that the fluid be set into motion by some external source such as a pump or fan, thus it can be seen that the pump or fan "forces" the fluid into motion (to flow through a tube) against its inertial and frictional forces.

Natural convection occurs when buoyance forces cause fluid motion. When a seemingly stationary fluid inside a tube is subjected to heat transfer through the tube walls, the fluid nearer to the tube walls would tend to heat up before the fluid in the centre of the tube. From the notion that fluid density tends to decrease with an increase in temperature, the fluid close to the tube walls will be less dense than the fluid in the centre of the tube. The effect of buoyancy will then see the fluid at the tube walls rise up and the fluid in the centre of the tube sink downward. This buoyancy induced motion is what is known as secondary flow and can contribute to the heat transfer coefficient in the tube.

Mixed convection refers to the mode of heat transfer where forced and natural convection play a significant role [24]. Forced convection can easily overpower natural convection when a pump or a fan is driving the flow. Mixed convection can only occur when the extent of fluid mixing caused by buoyancy forces is comparable to the extent of fluid mixing caused by the movement of the fluid induced by the pump or fan.

When considering fluid flow through a horizontal, circular tube, forced convection would tend to dominate when the fluid flows at high velocities and thus secondary flow effects can be neglected completely. Only at very low Reynolds numbers (early laminar flow regime) can secondary flow have a noticeable effect on the flow dynamics and thus the heat transfer coefficient inside the tube.

2.2.4. GRASHOF NUMBER

The Grashof number, a dimensionless parameter, is used to categorise flow regime during natural convection. According to Çengel and Ghajar [2] the Grashof number is the ratio of the buoyance force to the viscous force acting on a fluid during natural convection heat transfer. The Grashof number for circular tubes can be calculated using Equation 2.9.

$$Gr_L = \frac{g\beta(T_s - T_\infty)d^3}{v^2} \quad [2.9]$$

The Prandtl number is a dimensionless parameter that represents the ratio between the molecular diffusivity of momentum and the molecular diffusivity of heat. It is also used to describe the relative thickness of the velocity and thermal boundary layers [2]. The Prandtl number can be calculated using Equation 2.10:

$$Pr = \frac{v}{\alpha} = \frac{\mu C_p}{k} \quad [2.10]$$

The Rayleigh number, the product of the Grashof and Prandtl numbers, is a dimensionless parameter that can be used to categorise the flow when dealing with forced or mixed convection.

$$Ra = Gr \cdot Pr \quad [2.11]$$

The Rayleigh number can be very useful when investigating flow inside tubes subjected to heat transfer, since its value can be used as a guideline in deciding whether secondary flow effects are prominent or negligible.

2.2.5. THE CHILTON - COLBURN ANALOGY

The dimensionless Nusselt number, named after Wilhelm Nusselt, is considered to be the dimensionless convection heat transfer coefficient. It represents the ratio between convection and conduction heat transfer and can be calculated using the following equation:

$$Nu = \frac{hd}{k} \quad [2.12]$$

The Reynolds analogy is commonly used to relate friction, heat transfer and mass transfer coefficients when the Prandtl number and Schmidt number ($\frac{\mu}{\rho D}$) are close to one. This analogy proved very convenient, but would be much more useful if it could be used for a greater range of Prandtl numbers. Chilton and Colburn [25] suggested a modified form of the Reynolds analogy which could be used for Prandtl numbers ranging from 0.6 to as high as 60, and Schmidt numbers between 0.6 and 3 000. The Chilton-Colburn analogy that relates the friction coefficient to the heat transfer coefficient can be expressed as in Equation 2.13.

$$f = \frac{Nu}{2 \cdot Re \cdot Pr^{1/3}} \quad [2.13]$$

2.2.6. FULLY DEVELOPED FLOW

When considering fluid flow through a tube under diabatic conditions, a thermal boundary layer is formed due to the temperature difference in the radial direction of the fluid. The thermal boundary layer thickness increases in the radial direction as the flow moves further downstream of the tube inlet. At the point where the thermal boundary layer reaches the centre-line of the tube, the flow is said to be thermally fully developed, since the boundary layer stays constant downstream of this point. In the fully developed region of a tube, both the friction factor and convective heat transfer coefficient remain constant down the length of the tube. The

section of the tube upstream of this point is known as the thermal entrance length, and is a function of the flow regime inside the tube. The thermal entrance length in the laminar and turbulent flow regimes can be calculated using Equations 2.14 and 2.15 respectively [2].

$$L_{T,lam} = 0.05 \cdot Re \cdot Pr \cdot d \quad [2.14]$$

$$L_{T,turb} = 10 \cdot d \quad [2.15]$$

Similar to the thermal entrance length, a hydrodynamic entrance length exists when fluid enters a tube. The hydrodynamic boundary layer forms due to the velocity difference in the radial direction of the fluid. However, since the Prandtl number of water is greater than 1, the thermal entrance length will always be greater than the hydrodynamic entrance length. Therefore, the flow is said to be fully developed downstream of the thermal entrance length of the tube.

2.2.7. TRANSITION

In 1883 Osborne Reynolds published work on fluid flow inside tubes and the existence of laminar and turbulent flow regimes [26]. His work then led to further research by Moody [27] who created a friction factor plot which we now know as the Moody diagram. The Moody diagram gives the friction factors for smooth and rough tubes as function of Reynolds numbers and also broadly defines on the diagram the different flow regimes of laminar, transition, and turbulent flow. Although the laminar and turbulent flow regimes are well defined, the transitional flow regime (especially the start and end of transition) is not well defined. However, the transitional flow regime can in general be defined as the flow regime where the flow changes from fully laminar to completely turbulent. Its Reynolds number range is affected by many factors such as tube roughness, inlet effects and even heating.

In the laminar flow regime the heat transfer coefficient is rather low due to a lack of fluid mixing. However, the pressure drop is also low in this regime which is beneficial in terms of required pumping power. During laminar flow the friction factor is proportional to $Re_x^{-0.5}$ and the heat transfer coefficient proportional to $Re_x^{0.5}$ [4]. In the turbulent regime exactly the opposite is true, the heat transfer coefficient is high and so is the pressure drop. In this regime the friction factor is proportional to $Re_x^{-1/5}$ and the heat transfer coefficient proportional to $Re_x^{4/5}$.

When it comes to the design of heat exchangers efficiency is important, thus the heat transfer coefficient and pressure drop both play a role. This optimum point between pressure drop and heat transfer coefficient can, in some cases, reside in the transition region.

2.2.8. INLET GEOMETRIES

Experimental studies have proved that the inlet condition to a tube can affect the transitional flow regime [8-14, 28]. Certain inlets tend to induce more turbulence than other inlets, thus affecting the start and end of transition. This section aims to give the reader a physical representation of the different inlet geometries that have been investigated; the findings of these investigations are discussed in more detail in Section 2.3.

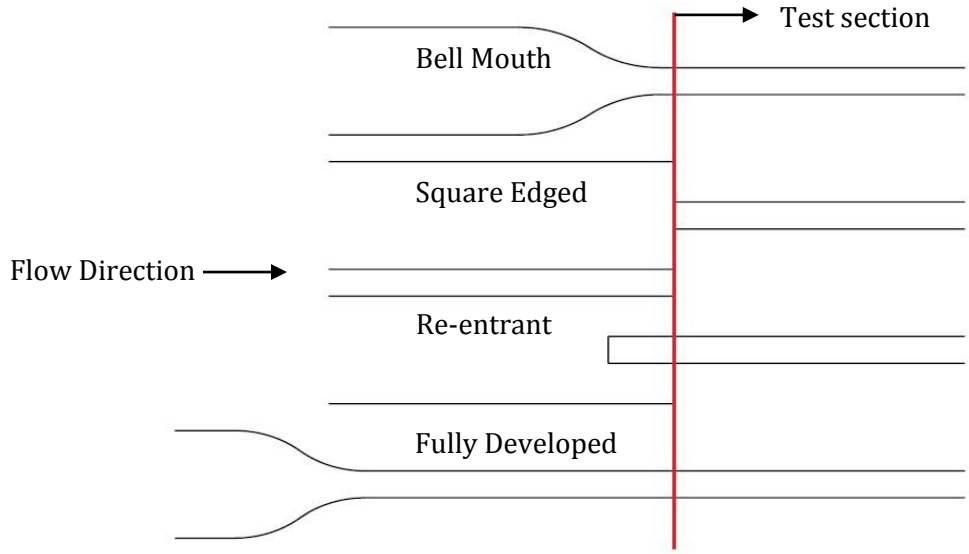

Figure 2.1: A schematic illustration of the different inlet configurations often used during experimental research into the transitional flow regime.

Bell-Mouth

The bell-mouth geometry is the smoothest transition from a large tube to a smaller tube. This is the inlet condition that was found to induce the least amount of turbulence, thus delaying transition the most.

Re-Entrant

The re-entrant inlet geometry caused the most turbulence at the entrance, thus delaying transition the least.

Square-Edged

The square-edged inlet geometry falls somewhere between the previous two when it comes to turbulence and the start of transition. This inlet is the most basic way of attaching a small tube to a larger section.

Fully Developed

When flow is studied far from the chosen inlet geometry the boundary layer has time to develop and the flow is categorised as fully developed. This way the inlet geometry has a much smaller impact on the flow conditions. Depending on where heating starts, the flow might be thermally and/or hydrodynamically fully developed.

2.2.9. SHELL-AND-TUBE HEAT EXCHANGERS

Shell-and-tube heat exchangers are the most common heat exchangers seen in industry. Their simple yet effective design has stood the test of time. They are used in many different formats, from condensers to boilers. A shell-and-tube heat exchanger consists of a shell, which can be under pressure, and a tube bundle that runs through the shell. The shell often has baffles that direct the flow over the tubes and encourages better fluid mixing of the shell-side fluid. The shell-side fluid never comes into direct contact with the tube-side fluid, thus all the heat transfer is directed through the tube walls. The Tubular Exchanger Manufacturers Association, Inc. (TEMA) provides international standards for the design of shell-and-tube heat exchangers [29].

The design of the heat exchangers can usually be broken down into the tube-side design and the shell-side design. The research in this paper concentrated on the tube-side flow, and thus the tube-side design of the heat exchanger.

The tube-side design mainly looks at the headers, the tube size, spacing and the tube configuration. The design of the headers affects the flow distribution (through the tube bundle) significantly and experimental as well as theoretical research has been done on this topic (see Section 2.4). The tube layout is an important design consideration for the shell-side as well as the tube-side; the possible layouts are presented in Figure 2.2. On the tube-side the tube configuration could affect the flow uniformity as well as the inlet condition to the tubes. On the shell-side the tubes need to be cleaned periodically to remove scale build-up and decrease the heat transfer resistance. Only the square and rotated square configurations can be cleaned using the conventional mechanical cleaning, the other configurations only have the option of chemical cleaning [30].

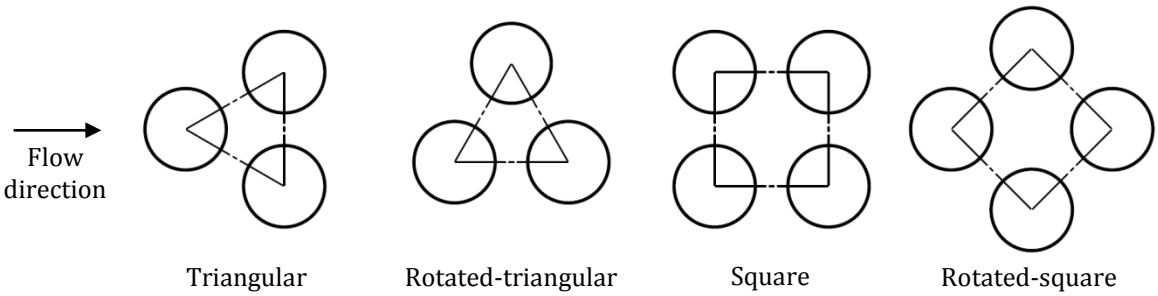

Figure 2.2: Schematic representation of the different tube layouts found in shell-and-tube heat exchangers [30]. The flow direction shown refers to the flow on the shell-side of the heat exchanger since the tube-side flow is along the tube length.

In terms of the tube pitch, most design guides suggest that a minimal tube pitch of 1.25 times the outer diameter of the tubes be used [30]. The reason for this value also stems from the need for mechanical cleaning. If the tube pitch is too small, the cleaning lanes between the tubes are too small. The benefits of using a smaller pitch seem obvious. Firstly a smaller pitch would allow for a more compact heat exchanger. Secondly a denser tube bundle should induce more turbulence on the shell side, leading to a larger heat transfer coefficient.

2.2.10. MALDISTRIBUTION IN HEAT EXCHANGERS

Maldistribution is an often occurring problem in shell-and-tube heat exchangers. On the tube side of a shell-and-tube heat exchanger the fluid normally enters from a single source before splitting into the numerous tubes with the help of an inlet header, as shown schematically in Figure 2.3. A uniform distribution of flow through all the tubes would be the ideal case since this would allow for the most efficient and compact design of the shell-and-tube heat exchanger. However, this is not always the case, the phenomenon of the fluid distributing non-uniformly is known as maldistribution and it has many negative effects.

It has been found that the heat transfer performance of the heat exchanger is not greatly affected by maldistribution [30]. This happens because of the fact that while some tubes encounter a low flow rate, others host a high flow rate, so the decrease in heat transfer coefficient in some tubes are countered by the increase thereof in other tubes. However, maldistribution has the drawback of making the performance of the heat exchanger unpredictable, which makes it difficult to design an efficient heat exchanger for a specific problem.

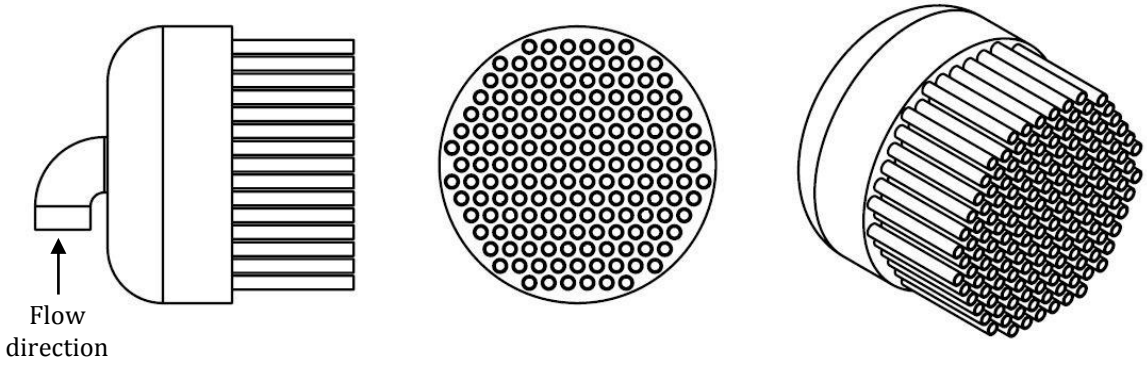

Figure 2.3: Schematic representation of an inlet header which serves the purpose of distributing the flow from a single source to multiple tubes.

In heat exchangers with high temperatures on the shell-side maldistribution could cause boiling of the tube-side fluid in the tubes where the flow rate is lower than desired. This would be highly unwanted as it could give rise to large performance losses as well as increased corrosion and possible overheating of the tube material.

The severity of maldistribution is affected by many design parameters. The inlet header serves the function of separating the fluid flow into the various tubes and thus has a large effect on maldistribution. A properly designed inlet header could render maldistribution negligible [5-7]. The pressure drop through the tube section also affects the degree of maldistribution, with a higher pressure drop causing less maldistribution. The pressure drop through the tube side would ideally be minimised since this would minimise pumping power required, thus the inlet header design would be a better parameter to vary for the sake of maldistribution.

2.3. THE TRANSITIONAL FLOW REGIME FOR HORIZONTAL CIRCULAR TUBES

The leading researchers in the field of transitional flow at tube inlets are Professor Ghajar from Oklahoma State University, and Professor Meyer, from the University of Pretoria. Although they have studied the effect of many variables on transition, all of their work has involved only single-tube heat exchangers (or test-sections as they are called in experimental investigations). The applicable work of Ghajar, Meyer and their respective colleagues are summarised in this section. Many of the studies included heat transfer data, however, only the friction factor findings relate to this study and the heat transfer findings will be neglected.

2.3.1. GHAJAR AND CO-WORKERS

Ghajar and his co-workers investigated fully-developed pressure drop characteristics in horizontal circular tubes operating in the transitional flow regime under adiabatic and diabatic conditions. In all cases discussed here the working fluid used was water-glycol mixtures with high Prandtl numbers and a constant heat flux was used as the heating mode (Diabatic investigations). Most of the studies used smooth tubes, though the investigations into enhanced tubes are also discussed briefly.

2.3.1.1. Studies using smooth tubes:

The experimental studies done by Tam and Ghajar [10], Tam *et al.* [9] as well as Ghajar and Madon [8] investigated the effect of varying inlet geometries (see Section 2.2.6.) on

the friction factor in the transitional flow regime. The first two studies also looked at the effect of heat transfer (diabatic conditions), while the last only investigated adiabatic conditions.

2.3.1.1.1. Adiabatic results

To investigate the effect of different inlet geometries on the adiabatic friction factor transition region, all three studies made use of an isothermal experimental set-up, varying the Reynolds number from fully laminar to fully turbulent flow. Three different inlet conditions were investigated, namely; re-entrant, bell-mouth and square-edged. An illustration of some of the inlet geometries considered is shown in Figure 2.1 (Section 2.1.6).

The results from all three studies showed that the change in inlet geometry affects the friction factor transition region significantly. Table 2.1 summarises the findings of all three studies in terms of the start and end of the transition region for the different inlets during adiabatic conditions:

Table 2.1: The effect of inlet geometry on the start and end of the transitional flow regime during adiabatic conditions.

	Transition region "start – end" [Re]		
	Re-entrant:	**Square-edged:**	**Bell-mouth:**
Tam and Ghajar [10]	2 870 – 3 500	3 110 – 3 700	5 100 – 6 500
Tam *et al.* [9]	2 032 – 3 031	2 222 – 3 588	Not Applicable
Ghajar and Madon [8]	1 980 – 2 600	2 070 – 2 840	2 125 – 3 200

From the table it follows that the re-entrant inlet configuration caused the most disturbance in all cases, thus aggravating transition the most, followed by the square-edged and then the bell-mouth inlets.

2.3.1.1.1. Diabatic results

Tam and Ghajar [10], as well as Tam *et al.* [9] included the effect of heat transfer to the fluid into their investigations. A constant heat flux boundary condition was used as the heating method in both cases, however, only the first study investigated different heat flux values. The second study stated that a uniform average flux was applied ranging from 4.3 to 8.9 kW/m^2. The diabatic results from both studies are summarised in Table 2.2:

Table 2.2: The effect of inlet geometry on the start and end of the transitional flow regime during diabatic conditions.

		Transition region "start – end" [Re]		
	Heat Flux: [kW/m^2]	**Re-entrant:**	**Square-edged:**	**Bell-mouth:**
Tam and Ghajar [10]	3	3 060 – 3 890	3 500 – 4 180	5 930 – 8 730
	8	3 350 – 4 960	3 860 – 5 200	6 480 – 9 110
	16	4 090 – 5 940	4 450 – 6 430	7 320 – 9 560
Tam *et al.* [9]	4.3-8.9	2 257 – 3 250	2 316 – 3 941	Not Applicable

It was found that in the lower parts of the transition region heating had a much greater effect on the fully developed friction factor since secondary flow can play a more prominent role in the flow dynamics at lower Reynolds numbers (lower average fluid velocity). As soon as turbulence starts, the effects of secondary flow are overpowered. When considering the results as depicted in Table 2.2 it can be concluded that an increase in heat flux delays the start of the transitional region for all inlet conditions, thus the lower and upper limit of the transition region would occur at higher Reynolds numbers when heat is transferred to the fluid.

In both these studies the inlet configuration had the same effects on transition for adiabatic and diabatic conditions. However, the friction factor results in the laminar flow regime showed contrasting behaviour. Tam and Ghajar [10] stated that heating increased the fully-developed friction factor in the laminar flow regime while Tam *et al*. [9] stated the opposite effect. The reason for this anomaly was not addressed.

The results from both studies showed that heating had a negligible effect on the fully-developed friction factor in the turbulent flow regime, with all their results correlating well to the Blasius equation (see Section 2.2).

2.3.1.2. Studies using enhanced tubes

A study done by Tam *et al.* [28] was very similar to the study of Tam *et al.* [9] (discussed in Section 2.3.1.1) except that enhanced tubed were used with varying spiral angles. Experiments were done under adiabatic and diabatic conditions with square-edged and re-entrant inlet profiles used.

Their results showed the start of transition to be dependent on the inlet profile, spiral angle and heat flux. An increase in spiral angle proved to encourage the start of transition while an increase in heat flux delayed the start. However, the end of transition proved to be solely dependent on the spiral angle of the enhanced tubes.

The enhanced tubes showed an increase in friction factor for all flow regimes during diabatic and adiabatic conditions when compared to smooth tubes. This was attributed to the resistance caused by the fins at the tube wall.

2.3.2. MEYER AND CO-WORKERS

Meyer and his co-workers also investigated the transitional flow regime for horizontal circular tubes (smooth and enhanced) in both adiabatic and diabatic conditions. The main difference between the work of Meyer and the work of Ghajar lies in the fluid used in the experiments. Meyer and his co-workers made use of water (Pr ≈ 6) as the working fluid while the studies of Ghajar discussed in Section 2.3.1 made use of a water-glycol mixture with much higher Prandtl number ranges (Pr ≈ 20).

2.3.2.1. Studies using smooth tubes

The study done by Olivier and Meyer [14] investigated the effect of inlet geometry and heat transfer on the transitional flow regime inside smooth copper tubes. Water was used as the working fluid and a constant surface temperature boundary condition was used to create diabatic conditions. The water was cooled in this case and pressure drop measurements were taken over the fully-developed section of the tube.

2.3.2.1.1. Adiabatic results

Two different tube diameters were used during the experiments, 15.9 mm and 19 mm. The inlet profiles used were similar to the ones used by Ghajar and his colleagues as are shown schematically in Figure 2.1, this study also included the hydrodynamically fully developed inlet. Olivier and Meyer [14] compared their results to the work of Tam and Ghajar [10] and similarities were identified during adiabatic conditions, even though different working fluids and different heating modes were used. Once again the start of transition was highly dependent on the inlet geometry, with the smoother inlets delaying transition the most. It was also found that the diameter of the tube had an effect on the start of transition, specifically with the bell-mouth inlet geometry. The larger tube delayed transition more than the smaller tube; this was credited to the fact that the bell-mouth sections were slightly different for the two tube sizes. The effect of inlet geometry on the transition region was attributed to the turbulence induced by the inlet profile, the less turbulence created, the more transition is delayed.

2.3.2.1.2. Diabatic results

For the diabatic investigation a counter-flow tube-in-tube heat exchanger set-up was used, with distilled water as the working fluid. Heated fluid was pumped through the inner tube with cooled fluid surrounding it; this was done to create a constant wall temperature boundary condition. The cooler fluid in the annulus flowed with a high velocity, ensuring the wall temperature never varied by more than 3°C, thus establishing a near constant wall temperature boundary condition. The heat transfer rates were varied by varying the flow rate of the inner fluid, values ranged from 100 W to 15 000 W.

The diabatic results showed that inlet condition had no effect on the start of transition when using water as the working fluid. This is in contrast to the findings of Tam and Ghajar [10] and Tam *et al.* [9], but was attributed to the difference in working fluids (Prandtl numbers) between the two studies. The investigation by Olivier and Meyer [14] made use of water, while the investigations by Ghajar used a water-glycol mixture. Olivier and Meyer [14] concluded that secondary flow effects were strong enough to dampen the effects caused by the inlet profile.

Their results also showed that cooling of the fluid increases the friction factor significantly in the laminar flow regime. This outcome was also linked to the effects of buoyance-induced secondary flow. A similar study was done later by Meyer and Olivier [11] using only a single tube diameter. The results agreed with the earlier work and showed that diabatic conditions dampen the effect of inlet disturbances.

2.3.2.2. Studies using enhanced tubes

Meyer and Olivier [11, 12] investigated the friction factor inside enhanced tubes for laminar, transitional and turbulent flow. As in the previous studies discussed in this chapter, different inlet geometries were used in this investigation. An adiabatic and diabatic study was done for developing and fully developed flow conditions. The experimental set-up made use of a tube-in-tube heat exchanger in a counter flow configuration with water as the working fluid.

2.3.2.2.1. Adiabatic results

For the adiabatic investigation the annulus was not used, thus only the inner tube contained flowing water. The results were based upon the friction factor for increasing and decreasing Reynolds number. When comparing the friction factor results of enhanced tubes to that of smooth tubes the following was noticed:

- Enhanced tubes showed constantly higher values of friction factor in the laminar and turbulent regimes when compared to smooth tubes.
- Enhanced tubes tended to aggravate the start of transition compared to smooth tubes.
- The friction factor in the turbulent flow regime proved to be solely dependent on the helix angle of the enhanced tubes.
- There tends to be a second smooth increase in friction factor values for enhanced tubes at Reynolds numbers between 3 000 and 10 000, a so called “secondary transition”.

The constantly higher friction factors in the laminar and turbulent regimes, as well as the earlier transition, was attributed to the higher levels of roughness in enhanced tubes compared to smooth tubes. The so called “second transition” could be attributed to the helical fins inducing rotation in the fluid at higher flow rates. This would also explain the difference in friction factor values for different helix angles. Taking the second transition into account, these enhanced tubes only reached fully turbulent conditions at a Reynolds number of 10 000. Hysteresis was not noticeable, as was the case with the smooth tubes.

Inlet geometry effects on transition were investigated in the same way as with the smooth tubes. Bell-mouth, square-edged and re-entrant inlet geometries were used. Furthermore, as was the case with the smooth tubes, two different tube diameters were tested, 15.8 mm and 19 mm. The effect of inlet geometry was very clear in the 15.8 mm tube, with the bell-mouth

geometry delaying transition the most, followed by the square-edged and the re-entrant geometries respectively. The effects of inlet geometry were less noticeable in the 19 mm tube. It was also found that helix angle affects the end of transition more than the start; a greater helix angle causing higher turbulence and thus an earlier end to transition. The friction factor in the turbulent regime was found to be unaffected by the inlet geometries.

2.3.2.2.2. Diabatic results

As stated previously, the experimental set-up made use of a tube-in-tube heat exchanger in a counter flow configuration. For the heat transfer experiment the annulus was incorporated with cold water as the working fluid. The annulus was set up to have a high flow rate, this way a near constant wall temperature boundary condition could be achieved for the inner tube.

The friction factor results yielded interesting information with regard to the transition flow regime. As was the case with the adiabatic investigation, enhanced tubes showed an overall increase in friction factor. The results for the turbulent flow regime agreed with the results from the adiabatic investigation; with a secondary transition present between Reynolds numbers of 3 000 and 10 000. In the laminar flow regime there was a noticeable increase in friction factor caused by the cooling of the fluid.

It was also found that the inlet geometries have no effect on the start of transition when heat transfer is present; transition was found to occur between Reynolds numbers of 2 000 and 3 000 consistently. This finding disagreed with the work of Tam *et al.* [28]. However, the contrast in this particular result between the work of Ghajar and work of the Meyer was attributed to the fact that Meyer's work was done with water, while Ghajar made use of a water-glycol mixture. One can thus come to the conclusion that the Prandtl number will be a key factor in deciding whether the inlet geometry will affect the start of transition.

2.3.2.3. Studies using nanofluids

A study done by Meyer *et al.* [15] also investigated pressure drop characteristics for a smooth circular tube in the transitional flow regime. However, during this investigation nanofluids were used instead of plain water. Aqueous suspensions of multi-walled carbon nanotubes at varying concentrations were used as the working fluid. A constant heat flux of 13 kW/m^2 was applied to the tube wall for the diabatic tests.

This study used the adiabatic friction factor for plain water as validation. The results showed transition to lie in the Reynolds number range of 3 000 to 3 100. This delayed transition was attributed to inlet effects. The diabatic results also showed agreement to the Poiseuille and Blasius equations in laminar and turbulent flow respectively.

The diabatic results for plain water showed transition to start at a Reynolds number of 2 900 and end at 3 600. In the laminar flow regime the friction factors proved to be lower than the adiabatic case, agreeing with the work of Tam *et al.* [9]. The turbulent results showed the friction factors to be slightly lower than the adiabatic case. The turbulent friction factors were compared to the modified Blasius equation suggested by Allen and Eckert [23] (Section 2.2.2), however, the difference between the standard and modified equation proved to be negligible, even at a heat flux of 13 kW/m^2.

Diabatic nanofluid results showed that the concentration of the carbon nanotubes had a significant effect on the friction factors in the laminar flow regime. The higher concentration nanofluid showed much lower friction factors in laminar flow and also showed the earliest transition ($2\,300 < Re < 2\,400$). In the turbulent flow regime, the effect of the nanofluid concentration was similar but less prominent.

2.3.2.4. Developing flow

A recent study done by Everts [17], under supervision of Meyer, investigated the pressure drop characteristics for developing flow in the transitional flow regime. This study investigated adiabatic and diabatic conditions with constant heat flux values of 6.5, 8 and 9.5 kW/m^2.

The adiabatic results agreed with the work of Tam *et al.* [9] and Olivier and Meyer [14], even though the pressured drops were measured in the developing section of the flow. The laminar friction factors proved to be slightly higher than the fully-developed studies and the transitional flow regime showed a similar start but an earlier end (steeper transition).

The effect of heating was less pronounced in this study than in the studies of fully-developed friction factors. The results showed that the applied heat flux delayed transition, as was the case with the previous discussed studies. The laminar friction factors increased with an increase in heat flux. The early turbulent flow regime showed a decrease in friction factors when compared to the adiabatic case, however, this effect became less pronounced as the Reynolds number increased. In the early turbulent flow regime the diabatic results correlated well to the Allen and Eckert [23] equation.

2.4. FLOW MALDISTRIBUTION

This section contains a brief overview of some literature on flow maldistribution for horizontal circular tube bundles. Although maldistribution is not the aim of this investigation, maldistribution is an important factor to consider whenever flow is divided into multiple tubes.

A study done by Lalot *et al.* [6] investigated the effect of flow maldistribution in heat exchangers. An electric heater was used with various inlet header designs. The extent of maldistribution is often expressed as a velocity ratio (highest velocity in the tubes to the lowest velocity in the tubes), which can be roughly quantified by the following expression [31]:

$$\eta = \sqrt{\frac{\frac{1}{2}\rho V_0^2 + \Delta p_{avg}}{\Delta p_{avg}}} \qquad [2.16]$$

With $\frac{1}{2}\rho V_0^2$ the dynamic pressure in the inlet pipe and Δp_{avg} as the average pressure drop across the tubes. From this equation it follows that a larger pressure drop across the tubes would lead to less maldistribution. Lalot *et al.* [6] also proved mathematically that maldistribution would be more detrimental in electric heaters than in two-fluid heat exchangers such as a shell-and-tube heat exchanger.

This study investigated multiple inlet header geometries experimentally and numerically, with the help of CFD software. An empirical equation was developed to predict the velocity in any one of the tubes with the knowledge of the header dimensions. Furthermore, the results showed that reverse flow is a real possibility in poorly designed inlet headers. The numerical results showed that the diameter of the inlet tube as well as the header depth had a major effect on maldistribution. Different header geometries were created and tested in a CFD environment. Deeper headers with larger inlet tube diameters showed the best performance in terms of uniform flow distribution.

Lalot *et al.* [6] then proceeded to investigate the effect of adding a perforated grid inside the inlet header. The grid had holes of 4 mm in diameter that were spaced at a pitch of 6 to 9 mm. The experimental results showed that the grid could change the velocity profile from a value of 4 to a value as low as 1.5 (Equation 2.16). This was a particularly useful result, as inlet headers are usually required to be compact, thus limiting the depth. With the introduction of a grid, the maldistribution could be greatly reduced without the physical size of the inlet header changing.

Another study on flow maldistribution in tube bundles was done by Kim *et al*. [5]. They used three-dimensional CFD models to investigate different inlet header designs, with the goal being a uniform flow distribution to all the tubes. Four different designs were tested with the flow rate and the header length as additional variables. They found that by simply changing the direction of the inlet stream, flow distribution could be significantly improved.

The pressure drop across the inlet header of a heat exchanger is a very important design factor, since pressure drop is directly related to pumping power. The study by Kim *et al*. [5] also investigated the pressure drop through four inlet header designs with the aim of finding the most efficient solution. The conclusion was drawn that placing the inlet stream 90° to the flow direction of the tubes would yield the best solution in terms of flow distribution and pressure drop.

Wang *et al.* [7] also studied maldistribution in tube bundles. As was discussed before, a porous baffle inside the inlet header has shown to have a positive effect on flow uniformity. Wang *et al*. [7] focused their attention on the optimal design of this porous baffle using experimental and numerical techniques. They made use of particle image velocimetry to quantitatively measure the flow field inside the inlet header, with and without a porous baffle. They used CFD software to find the optimum design of the baffle in terms of the hole distribution and geometry.

Their results showed that, without the use of a baffle, reverse flow is a possibility in the outer tubes of the tube bundle. This agreed with the much earlier work of Lalot *et al.* [6]. As was expected, their results showed a large improvement on flow uniformity with the inclusion of a porous baffle to the inlet header. They also tested the effect of a curved porous baffle and found a slight improvement on the normal baffle. In this study the pressure drop over the header was not taken into account.

2.5. SUMMARY AND CONCLUSIONS

In this chapter some background theory was presented relating to this study. The relevant literature into the transitional flow regime was summarised as well as some studies on flow maldistribution in tube bundles.

From the literature followed that the transitional regime, for circular tubes, will be affected by the presence of heat transfer. An applied heat flux caused a delay in transition for all inlet geometries when using tubes with smooth inner walls. The effect of heat transfer was found to be most visible at low Reynolds numbers since buoyance induced secondary flow has a more prominent effect in the laminar and early transitional regimes.

The influence of inlet geometry on the transition region was evident for adiabatic conditions in all the literature. It was found that the smoother the inlet condition, the less the flow is disturbed and the larger the delay in transition. However, the work done by Meyer and co-workers showed that the inlet geometry had no effect on the transition region when heat transfer is evident; while the work done by Ghajar and co-workers showed the opposite. The conclusion was drawn that for diabatic conditions, the inlet geometries will have no effect on the transition region if the Prandtl numbers are relatively low.

The investigations into enhanced tubes also yielded important conclusions. Firstly the enhanced tubes showed higher friction factors throughout the Reynolds number ranges. Furthermore, the helix angle proved to have an effect on the start of transition of transition, with the larger helix angle provoking the start of transition. In all the investigations enhanced tubes showed a secondary transition before settling into the turbulent regime.

Maldistribution in heat exchangers has been studied both experimentally and numerically by different researchers. The inlet header design showed to be the largest contributor to flow uniformity. The literature showed that the depth of the header, as well as the inlet tube

diameter, played the largest role in flow uniformity. It was also found that adding a porous baffle halfway between the inlet of the header and the tubes could reduce maldistribution greatly without increasing the depth of the header. Studies also suggested that a curved baffle could more effective than a standard baffle. Furthermore, the literature found that a simple change in the position of the inlet tube could yield exceptional improvement on flow uniformity without increasing the pressure drop by much.

It can therefore be concluded again from literature that the inlet geometry, heat flux and type of working fluid (Prandtl number) will influence the pressure drop characteristics in the transitional flow regime. Furthermore, it is possible that shell-and-tube heat exchangers might operate in or close to the transitional flow regime. This operating condition can be due to changes in operating conditions, scaling, corrosion or inlet maldistribution. As the tubes of shell-and-tube heat exchangers are so closely spaced it can be expected that the flow through neighbouring tubes will influence the inlet flow field of a specific tube and will therefore also influence the transitional pressure drop characteristics.

3. EXPERIMENTAL SET-UP AND DATA REDUCTION

3.1. INTRODUCTION

The experimental set-up used in this investigation was built to ensure accuracy and repeatability in all tests and measurements. As this was a purely experimental investigation, the plant, test set-up and data acquisition system were all purposely designed and will be described in detail in this chapter. This chapter also contains details of the data reduction method as well as the experimental procedure used in this study. Lastly, the uncertainty analysis is explained and the results for all the uncertainties are presented.

3.2. EXPERIMENTAL SET-UP

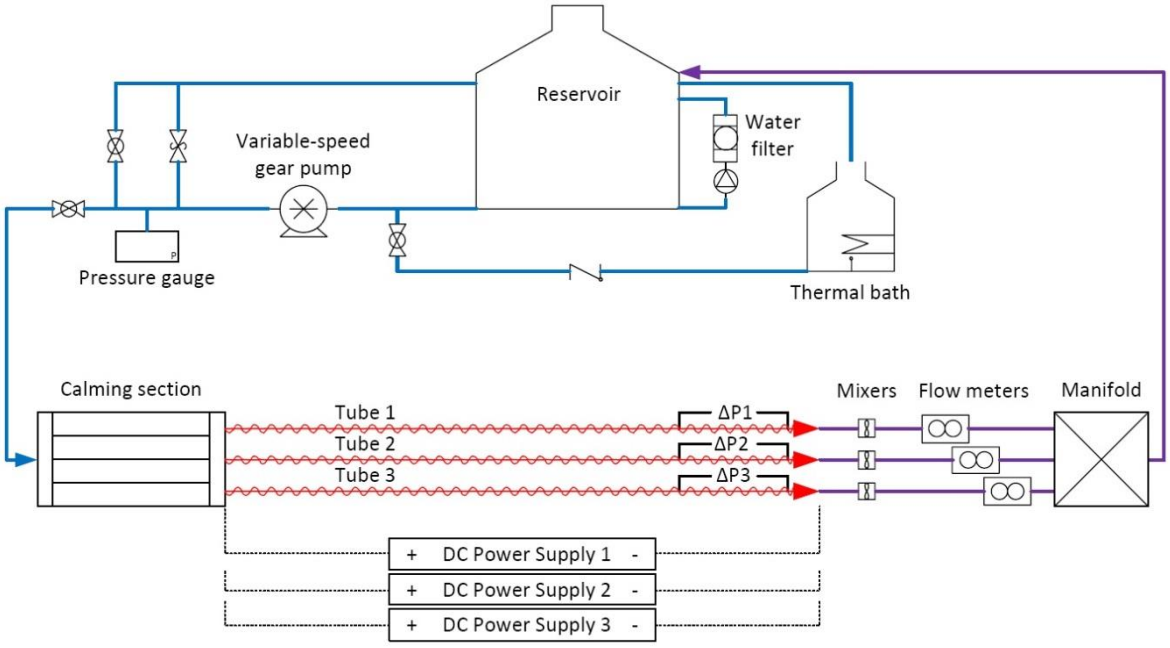

Figure 3.1: Schematic representation of the experimental set-up and triple-tube test section.

The layout of the experimental set-up and test section are shown schematically in Figure 3.1. The experimental set-up refers to the equipment and instrumentation used to transport and control the temperature of the working fluid, as well as the equipment and instrumentation needed to take the relevant measurements from the test section. The experimental setup shown schematically in Figure 3.1 was built from scratch as part of this study, photos of the experimental setup and the test sections are presented in Appendix A.

The test section refers to the heated tubes and acetyl inlet header that attaches the tubes to the calming section. Two test sections were built, a single-tube test section and a triple-tube test section. The triple-tube test section contains three tubes horizontally spaced at a pitch distance of 1.4 outer diameters. The measurements that had to be taken from the test section include: The inner wall temperature along each heat exchanger, the flow rate of the fluid through the heat exchanger and the pressure drop over the last 1.97 m of each tube. Thus every component was specified to operate effectively within the temperature, pressure and flow rate ranges that were to be investigated.

The experimental set-up made use of a closed loop system with water as the working fluid. An insulated reservoir with 1 000 litre capacity was used to store the water at a desired temperature. The temperature of the water was controlled by a thermal bath (900 W cooling

capacity) with an accuracy of ±0.1°C. The thermal bath was connected to ensure that it can either circulate water between the reservoir and itself, or provide water directly to the main pump and thus the test section. All experiments were conducted with an inlet water temperature of 22.5°C. The laboratory that housed the experimental set-up was continuously air-conditioned and was kept to a temperature of 22.5°C (±0.5°C). This ensured a stable thermal and operating environment for all material, equipment and instrumentation.

A separate filtration loop was added to ensure that any solid particles larger than 100 μm would be removed from the working fluid. A variable speed gear pump was used to control the mass flow rate of the water through the test section. A bypass valve was installed downstream of the pump to control the back pressure at the pump head. The bypass valve together with pump speed control made it possible to minimise the flow rate fluctuations through the test section.

Upstream of the test section a calming section was attached. The combination of the calming section and the acetyl inlet header to the tubes allowed for variation in the type of test section that was investigated. At the exit of every tube a mixer and a coriolis mass flow meter was installed to measure the bulk exit temperature and mass flow rate. The three mixers and mass flow meters were specified to be identical to ensure that the pressure drop through each tube be identical. A manifold at the exit of the three tubes ensured that the pressure drop due to outlet effects would be identical between the tubes before the flow was circulated back into the reservoir. The experimental set-up was operated to ensure that the outlet temperature of the water never exceeded 60°C, which was an operating limitation for the manifold.

3.3. CALMING SECTION

A calming section (Figure 3.2) was added upstream of the test tubes, its function was threefold. Firstly to direct the flow to the test section inlet. Secondly to reduce the turbulence levels in the water at the inlet of the test section. Thirdly to provide a square edged entrance profile to the inlets of the test section tubes, for both the single-tube and triple-tube test sections. The calming section was designed to bolt onto the inlet header of the test section. Acetyl was used as material for the inlet header/cap to prevent axial conduction as the thermal conductivity of acetyl is very low (0.36 W/mK).

The calming section geometry was kept as close to the design of Tam *et al*. [9] as possible, with the inner diameter increased due to three tubes being tested instead of just a single. The reasoning behind this was to ensure that the results would be comparable. In the literature a contraction ratio (calming section diameter divided by tube diameter) of 11.1 was used. For this study the contraction ratios were 12 and 62.5 for the triple-tube and single-tube test sections respectively.

To get the equivalent diameter for the triple-tube test section the total distance was used across the inlet of the three tubes, as is shown schematically in Figure 3.2.

The calming section was manufactured from clear acrylic plastic with an inner diameter of 250 mm and a length of 600 mm. The inside of the calming section contained three perforated acrylic plates (open air ratio of 0.31), a soda straw section and wire mesh. The wire mesh had an open air ratio of 0.65 and wire diameter of 0.3 mm.

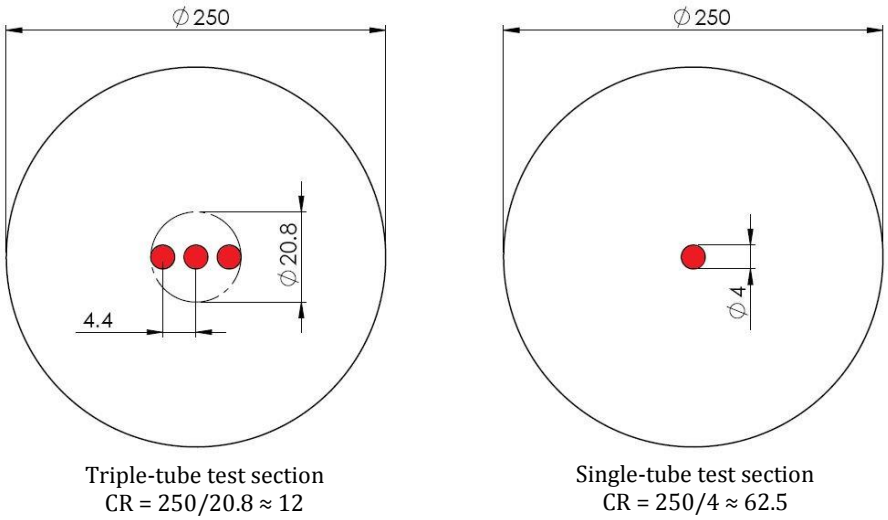

Figure 3.2: Schematic representation of the acetyl end-caps for both test sections showing the equivalent contraction ratios, with all dimensions in millimetres. The equivalent diameter of disturbance used for the triple-tube test section was 20.8 mm.

The calming section was also fitted with a PT100 thermocouple to allow for accurate measurement of the inlet water temperature to the test section. The calming section was insulated from the environment with 40 mm of insulation material with a thermal conductivity of 0.036 W/mK. One dimensional heat transfer calculations showed that this thickness was adequate to prevent heat loss to the environment.

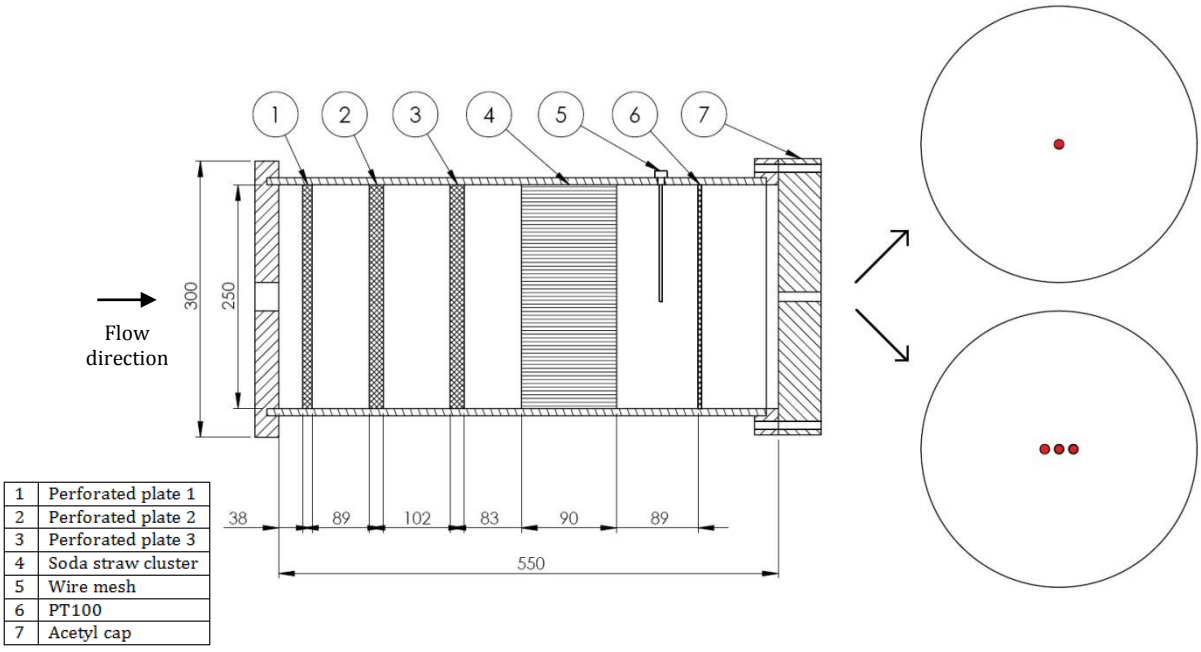

Figure 3.3: Cross-sectional view of the calming section showing all the inserts and the acetyl caps for both test sections (single-tube and triple-tube test sections). All dimensions in mm.

3.4. TEST SECTIONS

The test sections consisted of either one or three stainless steel tubes mounted directly into the acetyl inlet header to form a square edged inlet condition. The two test sections that were used in this study will be referred to as the single-tube test section and the triple-tube test section respectively. Each tube had an inner diameter of 3.97±0.01 mm measured with a split ball

measuring device and a micrometre at both ends of the tube. Each tube had a total length of 6.000 m (±1 mm). The outer diameter was measured as 6.00±0.01 mm using a micrometre. A constant heat flux was applied to each tube along the full length by running an electrical current through the tube itself. In this study the three tubes of the triple-tube test section will be referred to as Tube 1, Tube 2 (Centre-tube) and Tube 3. Tube 1 being the right side tube, when facing the direction of the flow, and Tube 2 as the Centre-tube (as indicated in Figure 3.1). The tube of the single-tube test section will be referred to as the Single-tube, when comparisons are made between the different tubes.

The electrical current running through each stainless steel tube induced the constant heat flux that heated the water as it flowed through the tube. The stainless steel measured an electrical resistivity of 72 μΩcm. Taking the length and cross-sectional area of the tube into account, the final electrical resistance was calculated to be 0.275 Ω from:

$$R_{tube} = \frac{\varepsilon L}{A_{cs}} \quad [3.1]$$

From this result a power supply could be selected to deliver sufficient current through the tube material to deliver a prescribed heat flux through the walls of the tube. The tubes were heated over the full length since the flow needed to develop thermally as well as hydrodynamically. At a Reynolds number of 2 300 the distance required for fully developed forced laminar flow is 3.21 m. As the heated length was 6 m, the selected tube length ensured that fully-develop flow will occur in approximately the last 2.79 m of the tube.

The pressure drop was measured over the last 1.97 m of the tube, which ensured that the flow was fully developed in the laminar flow regime. In the turbulent flow regime the development length is only 10 diameters or 39.7 mm, thus the placement of the pressure taps ensured only fully developed pressure drop measurements in all flow regimes.

The test sections were insulated to ensure minimal heat loss to the environment during testing. An insulating layer (thermal conductivity of 0.036 W/mK) of 80 mm was installed between the tube and the environment. One dimensional heat transfer calculations showed that during all experimental conditions the average heat loss to the environment would be less than 5%, while the maximum heat loss at certain operating condition (very low Reynolds numbers which were not relevant to this study) to the environment was less than 10%.

3.5. MIXERS

To accurately measure the average fluid temperature at the outlet of each tube, especially during laminar flow conditions, the water was mixed thoroughly to remove thermal stratifications. The mixers were designed based on the work of Bakker *et al.* [32], who investigated static mixer performance in the laminar flow regime. Each mixer consisted of a 9.5 mm copper tube with an insert of five splitter plates at 90° angles. Each plate had a length of 20 mm. The flow was thus split in half, cutting the boundary layer five times, thus mixing the fluid to ensure a zero thermal gradient in the radial direction. The mixer assembly included a PT100 thermocouple directly downstream of the final mixer plate to accurately measure the average fluid temperature at the exit of each tube. The mixers were installed 15 diameters downstream of the tube outlet and were connected by the use of rubber tubing on both sides to prevent axial conduction. A schematic representation of the mixer assembly that included the PT100 thermocouple is shown in Figure 3.4.

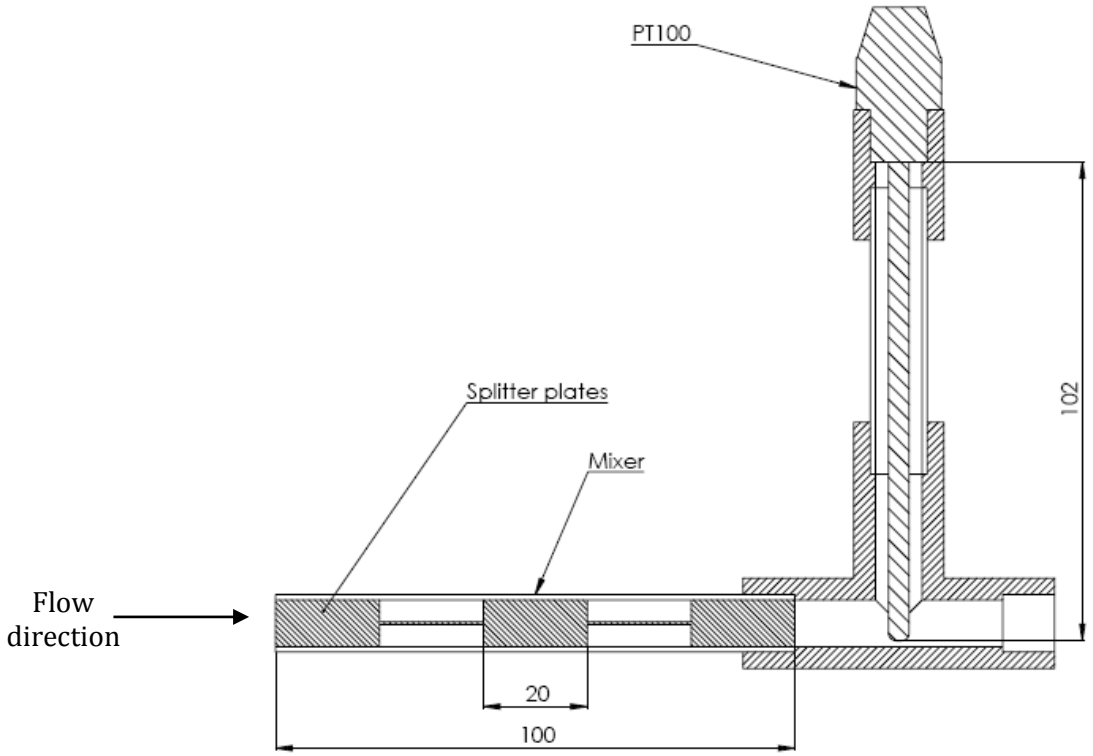

Figure 3.4: Mixer section with PT100 thermocouple attachment to measure the bulk fluid temperature downstream of each test tube. All dimensions are in mm.

3.6. MANIFOLD

A manifold was used at the exit of the triple-tube test section to unify the flow before returning back to the reservoir. Its purpose was to ensure that each tube had the same flow resistance.

Furthermore, as the three tubes were so closely spaced it was not possible to position the three mass flow meters at exactly the same distance downstream of the test section outlets. However, the three mass flow meters were of the same type and model and care was taken to ensure that the length and flow resistances of the downstream tubes were all the same. If the conditions for each tube leg were not exactly the same, as would be the case if the tubes were connected with elbows and T-sections, the resistance would differ for each tube which would negatively influence the outcome of this study. The manifold was designed to have the same inner diameter of the calming section (250 mm) and a length of 320 mm. Thus the design of the manifold was almost exactly the same as the calming section shown in Section 3.3 with the only differences being the length and the fact that the manifold had no inserts.

3.7. INSTRUMENTATION

3.7.1. POWER SUPPLIES

To provide a constant heat flux, each tube was connected separately to its own direct current power supply. The power supplies used were 1.5 kW units (Elektro-Automatic PS9040-60) capable of a maximum current output of 60 A within an accuracy of 0.2%. Since direct current was used as the heating mechanism (with the tube itself acting as an electrical resistor to build up heat), the power supplies were specified for high current output rather than high potential output. The power supplies also had built-in “sense” functionality, which allowed the power supplies to measure the amount of potential loss along the length of connecting cable and compensate therefor. Thus ensuring that the amount of power displayed on the power supply was the actual amount of power delivered to the test section. To minimise the effect of

electromagnetic interference the polarity of the Centre-tube was reversed to that of the outer two tubes. Furthermore, the connecting cables were covered by braided shielding.

3.7.2. FLOW METERS

Coriolis mass flow meters, manufactured by Micro Motion, were used downstream of each tube to measure the mass flow rate of the fluid. All three flow meters were exactly the same, with the capability of measuring to a maximum flow rate of 81.6 kg/h at an accuracy of 0.05% of the full scale.

3.7.3. PRESSURE TRANSDUCERS

To measure the pressure drop across the fully-developed section of each tube, pressure taps were drilled through the walls of the tubes at a diameter of 0.3 mm. Rayle [33] suggested that a hole of less than 10% the inner diameter of the tube will not affect the flow pattern, as was the case here. Furthermore, care was taken to remove any burrs caused by the drilling of the pressure tap holes.

Pressure transducers, manufactured by Validyne, were connected across the pressure taps to measure the differential pressure. The pressure transducers used had interchangeable membranes to ensure accurate measurement over a wide range of pressures. Three membranes were used during testing, a low-range membrane with a maximum pressure capability of 2.2 kPa, a mid-range diaphragm with a maximum pressure of 8.6 kPa and a higher-range membrane with a maximum capability of 22 kPa. All three membranes had an accuracy of 0.25% of their full scale values, leading to accuracies of 5.5 Pa, 21.5 Pa and 55 Pa for each membrane respectively.

3.7.4. TEMPERATURE MEASUREMENTS

PT100 thermocouple probes, manufactured by Omega, were used to measure the inlet and outlet temperature of the working fluid. The first PT100 was placed inside the calming section while the last PT100 was placed inside the mixer assembly, as shown in Figures 3.3 and 3.4 respectively. The PT100 probes were calibrated using a thermal bath with an accuracy of 0.03°C.

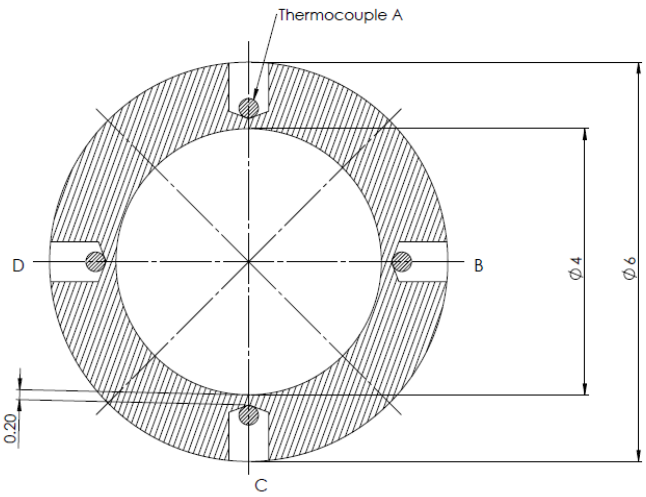

Figure 3.5: Cross-sectional view of the tube showing the thermocouple as mounted in the indentations, with the dimensions in mm. Each station only consisted of three thermocouples, with the left and right thermocouple being varied at each subsequent station.

Thermocouple stations were placed all along the tube length, with three thermocouples per station. At each station there was a thermocouple on the top and on the bottom of the tubes

(position A and C in Figure 3.5), with the third thermocouple positioned either on the left or the right side (positions D and B in the figure below). The position of the thermocouple on the side of the tube was alternated between left and right along the length of the tube. Figure 3.5 shows a cross-sectional view of the tubes at the position of a thermocouple station.

The indentations for the thermocouples were drilled into the tube wall to position the thermocouples as close to the inner wall of the tube as possible. With the distance along the length of each tube being x (x = 0 at the inlet of the tube) Table 3.1 gives the positions of the pressure taps and thermocouple stations.

Table 3.1: Positioning of the Pressure taps and thermocouple stations along the tube length. The distance, *x*, was measured from the inlet of the tube.

Measuring Point	Distance *x* [mm]
Thermocouple station 1	60
Thermocouple station 2	851
Thermocouple station 3	1 642
Thermocouple station 4	2 433
Thermocouple station 5	3 224
Pressure tap 1	4 000
Thermocouple station 6	4 015
Thermocouple station 7	4 291
Thermocouple station 8	4 569
Thermocouple station 9	4 846
Thermocouple station 10	5 123
Thermocouple station 11	5 400
Thermocouple station 12	5 678
Thermocouple station 13	5 954
Pressure tap 2	5 970

3.7.5. DATA CAPTURING SYSTEM

A data acquisition system was set up using a personal computer, a National Instruments SCXI system (signal conditioning extensions for instrumentation) and National Instruments Labview software. The Labview software was programmed to take measurements from the flow meters, the pressure transducers and the thermocouples; as well as being able to control the pump speed.

3.8. DATA REDUCTION

When a constant heat flux boundary condition is applied to a tube in which steady flow occurs, the average fluid temperature tends to increase linearly along the tube length, while the tube wall temperature shows a change in its gradient (Figure 3.6). This change in gradient indicates the transition point from developing to fully developed flow. In fully-developed flow the wall and fluid temperature increase with the same rate along the tube length since the heat transfer coefficient is constant.

With reference to Figure 3.6, the average bulk fluid temperature was calculated by taking a simple average between the inlet and outlet fluid temperatures as the temperature increase from inlet and outlet is linear.

$$T_b = \left(\frac{T_o + T_i}{2}\right) \quad [3.2]$$

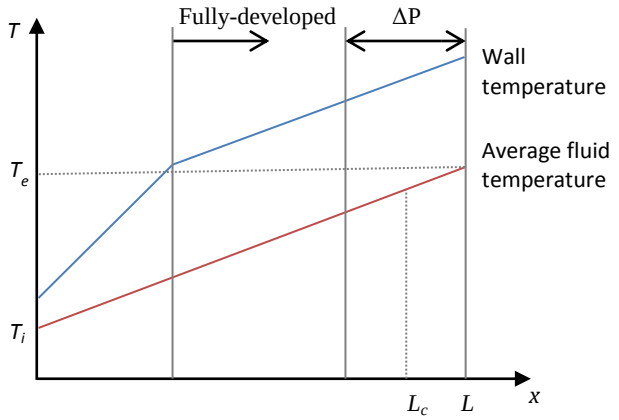

Figure 3.6: Schematic of average fluid temperature (red) and tube wall temperature (blue) along the length of tube with a constant heat flux being applied. Also shown is the section of tube where the pressure drop was measured during this study.

The average fluid temperature at any point, *x*, along the tube length was calculated using the gradient of the red curve in Figure 3.6.

$$T_m(x) = \left(\frac{T_o - T_i}{L}\right) x + T_i \qquad [3.3]$$

The average wall temperature of the tube was calculated using the trapezoidal rule.

$$T_w = \frac{1}{L}\int_0^L T_w(x)\, dx \qquad [3.4]$$

The thermophysical properties of the working fluid (water) were determined at the relevant temperatures by using the correlations suggested by Popiel and Wojtkowiak [34]. The water properties used in this study were density, viscosity, specific heat, conductivity and Prandtl number.

The Reynolds number of the flow between the two pressure taps (where the flow was always fully developed) was calculated using the following equation:

$$Re = \frac{4\dot{m}}{\mu d\pi} \qquad [3.5]$$

The properties used in the calculation of the Reynolds number were calculated at the average bulk fluid temperature between the two pressure tap locations, thus the average bulk fluid temperature over the last 1.97 m of each tube (distance L_c in Figure 3.6).

The average friction factors between the two pressure taps were determined from the measured pressure drops, mass flow rates, inner tube diameter, and distance between the two pressure taps. Again, the fluid properties were obtained from the temperature obtained between the two pressure taps, at distance L_c, as indicated in Figure 3.6.

$$f = \frac{\Delta p \rho d^5 \pi^2}{8\dot{m}^2 L_{pt}} \qquad [3.6]$$

The heat flux applied to each tube was determined from the electrical heating to the tube and the tube inner surface area.

$$\dot{q} = \frac{\dot{Q}_{electrical}}{A_s} = \frac{VI}{\pi dL} \qquad [3.7]$$

The electrical heating for each tube was equal to the measured product of the voltage supply and electrical current through the tube. The thermal energy transferred to the working fluid was calculated from the measured mass flow rate, fluid temperature rise of the water and the specific heat value at the average bulk fluid temperature (over the full heated length):

$$\dot{Q}_{fluid} = \dot{m} C_p (T_o - T_i) \quad [3.8]$$

The energy losses or energy balance errors (percentages) was defined as the difference between the electrical heating and thermal heat transfer to the water, with the electrical heating as reference.

$$EB = 100 \left| \frac{\dot{Q}_{electrical} - \dot{Q}_{fluid}}{\dot{Q}_{electrical}} \right| \quad [3.9]$$

As the test section was heated to a higher temperature than the air in the laboratory, and although the tests sections were well insulated, it was expected that the electrical input should always be higher than the heat transfer to the water stream because of small heat transfer losses to the environment. The experiments confirmed this, and the average energy balance of all experiments was 3.2%. The maximum energy losses of 5%, occurred at the lowest mass flow rates, when the water outlet temperatures and tube wall temperatures were highest. This was expected but had no influence on the outcomes of this study as it occurred during the lowest ranges of laminar flow, and not near the transitional flow regime which was the focus of this study. In the Reynolds number range of 2 000 to 4 000, all the energy balance errors were less than 3%.

3.9. EXPERIMENTAL PROCEDURE

Experimental data was collected over a Reynolds number range of 700 up to 6 500 for the single and triple-tube set-ups. This ensured that the laminar, transitional and turbulent flow regimes would be evident in the data. The Reynolds number of 6 500 was the maximum that could be achieved due to pressure limitations on the calming section.

The mass flow rate of the water was controlled in two ways. Firstly by controlling the speed of the pump itself and secondly by adjusting the position of the bypass valve. Incorporating the bypass valve enabled the pump to operate at a high speed and high back pressure even when a low flow rate was desired through the test section. This ensured minimal pulsations in the flow rate, especially in the laminar flow regime.

During the experimental testing, the flow rate was set to the desired value and the system was left to reach steady-state conditions. The pressure drop, temperature and mass flow rate measurements were plotted as a function of time to check that the conditions were at steady-state before measurements were taken. Measurements were only taken once no changes occurred for a period of at least 5 minutes. For a first experiment after the system was started up, it took approximately 120 minutes before steady-state conditions were reached, especially for laminar flow. Once steady-state conditions were achieved and measurements were taken, only small changes were made in the mass flow rates, after which steady-state conditions occurred after approximately 25 minutes.

At every measuring point, after steady-state conditions were achieved, 200 data points were collected for every signal (temperatures, pressure drops, mass flow rates, currents and voltages) at a sampling rate of 10Hz. The 200 data points were then averaged to form the raw data from every signal at the corresponding Reynolds number. Trials were done at higher and lower sampling frequencies; however, it was found that the measured data was independent of the sampling frequencies from 1 to 100 Hz. The results were also independent of the number of data points collected for the different sampling frequencies (trails were conducted with data points from 10 to 1 000 data points).

3.10. UNCERTAINTY ANALYSIS

The uncertainties of all measurements were either received from the suppliers of instrumentation or were estimated using the method suggested by Dunn [35] as was summarised by Everts [17]. A confidence interval of 95% was used throughout the calculations.

3.10.1. INSTRUMENTATION

3.10.1.1. Power supplies

Three identical power supplies were used to supply current to each tube. The manufacturer specifies an accuracy of 0.2% of the nominal value of current or voltage.

3.10.1.2. Mass flow meters

Three identical Coriolis mass flow meters with matching transmitters were used to measure the mass flow rate through each tube. The accuracies of these flow meters were 0.05% of the full scale value (1.36 kg/min), leading to a mass flow rate accuracy of $6.8x10^{-4}$ kg/min.

3.10.1.3. Pressure transducers

Differential pressure transducers with interchangeable diaphragms were used to measure the pressure drop in each tube. Three diaphragm sizes were used during testing, each with a maximum differential pressure of 2.2 kPa, 8.6 kPa and 22 kPa respectively. The smallest diaphragm was calibrated using a Betz manometer with a specified accuracy of 2.5 Pa. The other two diaphragms were calibrated with reference to a manometer of accuracy 25 Pa.

The uncertainty of each pressure transducer was calculated using the method summarised by Everts [17]. The pressure was increased in steps from 0 Pa to the full scale of each pressure transducer. The bias was taken as the accuracy of the manometer used for calibration and the precision was calculated from the data points that consisted of 200 readings at each step. The uncertainty of each pressure transducer is summarised in the table below.

Table 3.2: Summary of the uncertainty for each pressure transducer, calculated with the method suggested by Everts [17].

Pressure Transducer [kPa]	Uncertainty Range [Pa]
2.2	2.5 – 2.6
8.6	25.6 – 26.8
22	27 – 34

3.10.1.4. Thermocouples

The PT100 thermocouple probes were calibrated in a thermal bath with an accuracy of 0.03°C. The thermal bath temperature was varied from 10°C up to 65°C in 2.5°C increments. At every increment steady state was reached and 100 data points were collected for each thermocouple. The uncertainties of the PT100 temperature measurements were calculated in the same way as was done for the pressure transducers. The table below summarises the uncertainty values of each PT100 probe:

Table 3.3: Summary of the uncertainty for each PT100 thermocouple, calculated with the method suggested by Everts [17]. T0 was the probe used to measure the temperature in the calming section, and T1, T2, and T3 were used to measure the outlet temperatures of Tubes 1, 2, and 3 as indicated in Figure 3.1.

PT100 Probe	Uncertainty [°C]
T0	0.04
T1	0.04
T2	0.06
T3	0.04

3.10.1.5 Tube length and diameter

The tube length was measured with a measuring tape to an accuracy of 1 mm. The inner diameter of the tube was measured with a split ball measuring device and a micrometre. The micrometre had an accuracy of 20 µm.

3.10.2 FLUID PROPERTIES

The thermophysical properties of the working fluid, water in this case, were calculated at the relative temperature using the equations of Popiel and Wojtkowiak [34]. The uncertainties of these equations were determined and stated by the authors and are summarised in Table 3.4.

Table 3.4: Uncertainty summary for the thermophysical properties of water that was used as the working fluid [34].

Property	ρ [kg/m3]	µ [kg/m.s]	Cp [J/kg.K]	k [W/m.K]	Pr [-]
Uncertainty[%]	0.004	1	0.04	2	2.3

3.10.3. REYNOLDS NUMBER

From Equation 3.5 it follows that the uncertainty of the Reynolds number was dependent on the uncertainty of the mass flow rate, diameter, viscosity and cross-sectional area. Following the method of Everts [17], the uncertainty of the Reynolds number was calculated as follows:

$$Re = \frac{4 \cdot \dot{m}}{\mu \cdot D \cdot \pi} \qquad [3.5]$$

$$\delta Re = \left[\left(\frac{\delta Re}{\delta \dot{m}}\delta\dot{m}\right)^2 + \left(\frac{\delta Re}{\delta D}\delta D\right)^2 + \left(\frac{\delta Re}{\delta \mu}\delta\mu\right)^2\right]^{1/2} \qquad [3.10]$$

$$\delta Re = \frac{4}{\pi}\left[\left(\frac{1}{\mu \cdot D}\delta\dot{m}\right)^2 + \left(-\frac{\dot{m}}{\mu \cdot D^2}\delta D\right)^2 + \left(-\frac{\dot{m}}{\mu^2 \cdot D}\delta\mu\right)^2\right]^{1/2} \qquad [3.11]$$

Figure 3.7 shows the uncertainties of the Reynolds number values for the Single-tube and each tube of the triple-tube test section during diabatic conditions. These plots were produced by taking the uncertainties of the measuring equipment, as well as the standard deviation of 200 measurements (at steady-state conditions) into account.

The figure shows that the highest uncertainties lie in the region of transition from laminar to turbulent flow. The reason for this stems purely from the standard deviation of the measurements. During transitional flow the mass flow rate of the fluid is unstable, which leads to instability in all the dependent measurements, such as the pressure drop and the outlet temperature. The transitional flow regime has been described as orderly flow with flashes of turbulence [4], which would describe the unstable nature and thus the higher uncertainties in this regime.

Figure 3.8 shows two sets of 200 measurements taken from the flow meter connected to the single-tube test section. The first set of points was taken in the laminar flow regime and the second was taken while the flow was in transition. Even though both sets of data were taken at steady-state conditions the figure shows the signal to be more stable in the laminar flow regime, justifying the higher uncertainties in the transitional flow regime. However, the uncertainty of the Reynolds number remained below 5% for all the tubes and all flow conditions.

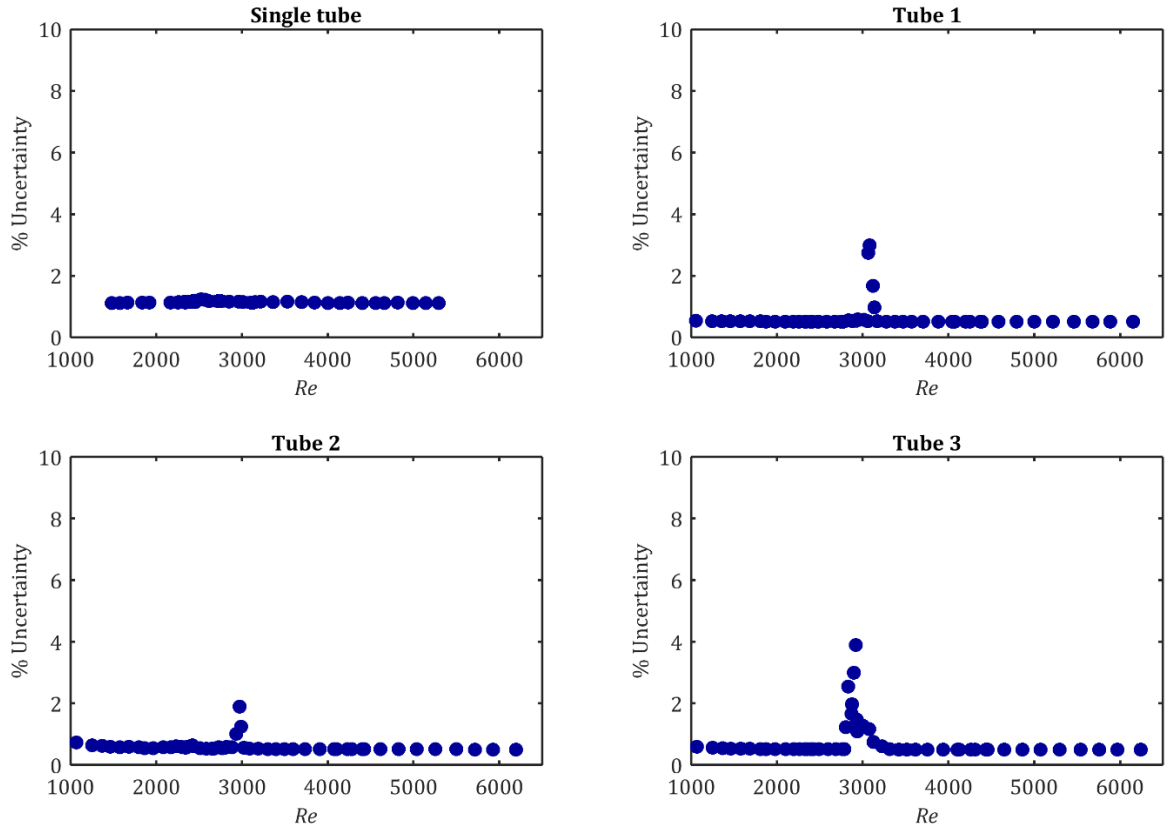

Figure 3.7: Percentage Reynolds number uncertainty as a function of Reynolds number for the single-tube test section and each tube of the triple-tube test section. A heat flux of 3 kW/m² was applied to each tube and all measurements were taken at steady-state conditions.

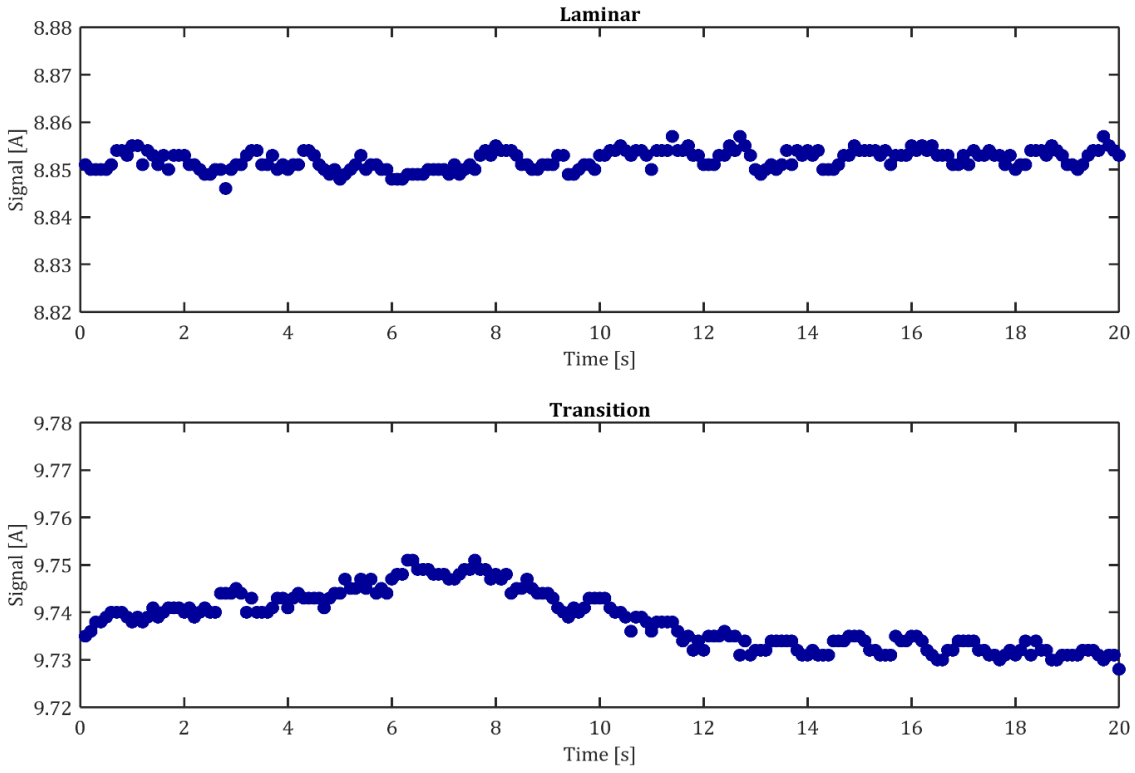

Figure 3.8: Two sets of 200 measurements from the same mass flow meter with the flow in the laminar flow regime in the first case and in the transitional flow regime in the second.

3.10.4. FRICTION FACTOR

The same method was followed to determine the uncertainty of the friction factor:

$$f = \frac{\Delta p \cdot \rho \cdot D^5 \cdot \pi^2}{8 \cdot \dot{m}^2 \cdot L_{pt}} \quad [3.6]$$

$$\delta f = \left[\left(\frac{\delta f}{\delta \Delta p} \delta \Delta p \right)^2 + \left(\frac{\delta f}{\delta \rho} \delta \rho \right)^2 + \left(\frac{\delta f}{\delta D} \delta D \right)^2 + \left(\frac{\delta f}{\delta \dot{m}} \delta \dot{m} \right)^2 + \left(\frac{\delta f}{\delta L_{pt}} \delta L_{pt} \right)^2 \right]^{1/2} \quad [3.12]$$

$$\delta f = \frac{\pi^2}{8} \left[\begin{array}{c} \left(\frac{\rho \cdot D^5}{\dot{m}^2 \cdot L_{pt}} \delta \Delta p \right)^2 + \left(\frac{\Delta p \cdot D^5}{\dot{m}^2 \cdot L_{pt}} \delta \rho \right)^2 + \left(\frac{5 \cdot \Delta p \cdot \rho \cdot D^4}{\dot{m}^2 \cdot L_{pt}} \delta D \right)^2 \\ + \left(-\frac{2 \cdot \Delta p \cdot \rho \cdot D^5}{\dot{m}^3 \cdot L_{pt}} \delta \dot{m} \right)^2 + \left(-\frac{\Delta p \cdot \rho \cdot D^5}{\dot{m}^2 \cdot {L_{pt}}^2} \delta L_{pt} \right)^2 \end{array} \right]^{1/2} \quad [3.13]$$

The results for the uncertainty of the friction factor are presented graphically in Figure 3.9. From these figures it follows that higher uncertainties reside in the area of transition, as was the case with the Reynolds number. Table 3.5 summarises the results of the uncertainty analysis of the single-tube test section as well as the triple-tube test section. It follows from the results that the uncertainties of the friction factors were in general a maximum of 3%, but uncertainties of up to 8% occurred in the transitional flow regime.

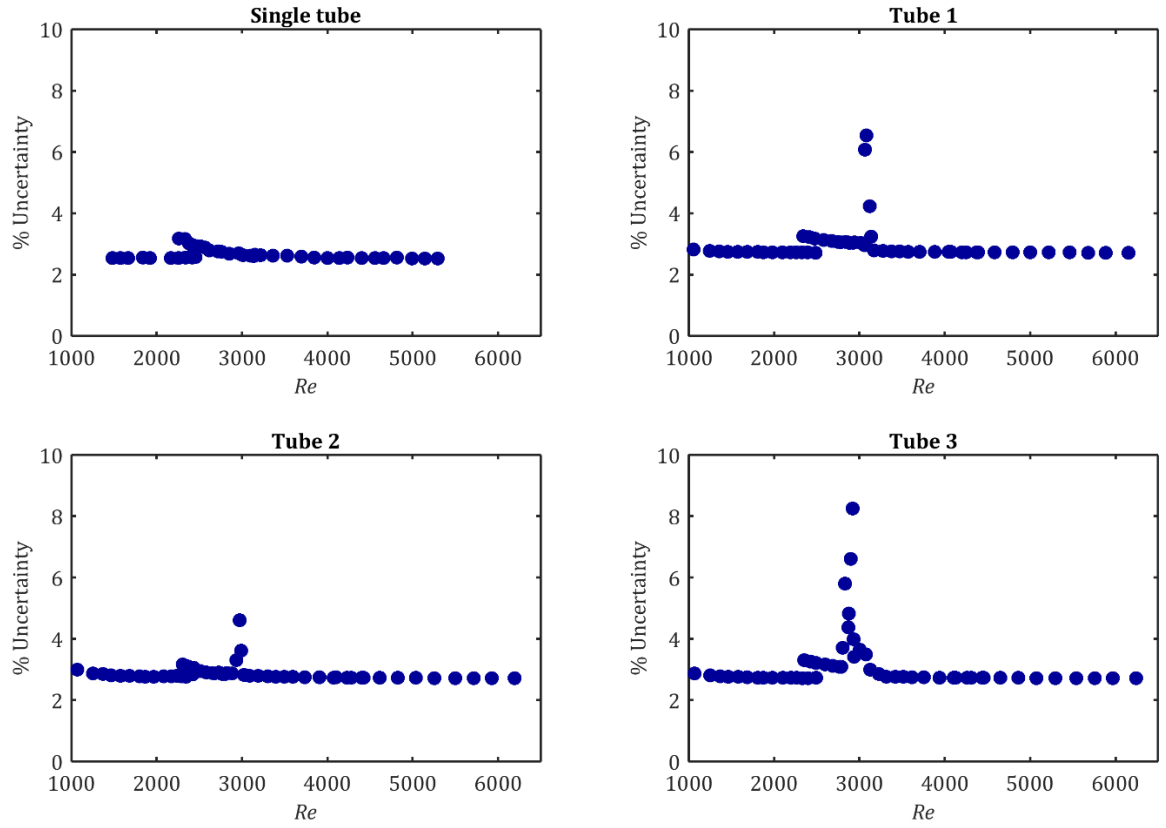

Figure 3.9: Percentage friction factor uncertainty as a function of Reynolds number for the single-tube test section and each tube of the triple-tube test section. A heat flux of 3 kW/m² was applied to each tube and all measurements were taken at steady-state conditions.

Table 3.5: Summary of the uncertainty percentages for the Reynolds number and friction factor for all the tubes used in this study.

		Single-tube	Tube 1	Tube 2	Tube 3
Reynolds number	Average [%]	1.15	0.63	0.60	0.78
	Max [%]	1.23	2.98	1.90	3.89
Friction factor	Average [%]	2.65	3.00	2.87	3.19
	Max [%]	3.17	6.53	4.61	8.25

3.11. SUMMARY AND CONCLUSIONS

The purpose of this chapter was to discuss the experimental set-up, experimental procedure, instrumentation, data reduction methodology and uncertainty analysis of this experimental investigation. A plant was designed and constructed that could accommodate two different test sections, either a single-tube or a triple-tube test section. Upstream of the test section was a calming section which was also used as an inlet for the circular tubes.

The tube diameters and tube lengths for all tubes were the same. The single-tube test section was used as the reference tube to validate the experimental set-up against previous studies. With the triple-tube set-up, a total of three tubes could be tested parallel to each other; also at the same heat flux and a squared edge inlet. These tubes were spaced 1.4 diameters from each other.

Stainless steel tubes were used with an inner diameter of 3.97 ±0.01 mm. The tubes were heated by direct current, each from its own power supplies; this ensured a constant heat flux of 3 kW/m^2 at the wall of each tube. The tubes were insulated from the environment to ensure minimal heat loss. The flow rate was measured using coriolis mass flow meters, one for each tube. The pressure drops were measured in the region of fully-developed flow using pressure transducers with variable diaphragms to ensure the highest possible accuracy. The inlet temperature to the tubes was measured by a PT100 thermocouple probe mounted inside the calming section. The outlet bulk fluid temperature was measured for each tube by adding a mixer containing a PT100 thermocouple to the outlet of each tube.

During testing the Reynolds number was varied from a value of 1 000 up to a value of 5 500. Thus the laminar, transition and turbulent flow regimes were visible in the data. At each flow rate increment the pressure drop and temperature conditions were checked for steady state before a measurement was taken. Each measurement consisted of 200 points taken at a frequency of 10 Hz, with these 200 points then averaged to give the raw measurement.

An uncertainty analysis was conducted on all the parameters evaluated in this study. It was found that the Reynolds number uncertainties in general were lower than 2%, except in the transitional flow regime where the uncertainty reached values as high as 5%. The same tendency was found for the friction factors; in general the uncertainties were lower than 3%, however, in the transitional flow regime a maximum of 8% was recorded.

4. VALIDATION

4.1. INTRODUCTION

The experimental set-up, data acquisition system and data reduction method was validated against existing experimental as well as theoretical data. Since this investigation focussed on the pressure drop characteristics in the transitional flow regime with a constant heat flux boundary condition, the diabatic friction factor was calculated and plotted as a function of Reynolds number. The single-tube test section was used to validate the experimental set-up and procedure, since similar work was published in literature that could be used for validation purposes.

4.2. DIABATIC FRICTION FACTOR

The single-tube test section was used to validate the experimental set-up and procedure. A constant heat flux boundary condition of 3 kW/m² was applied to the tube and fully-developed pressure drop measurements were recorded. The flow rate was decreased from a Reynolds number of 5 300 down to 1 500 to ensure that all three flow regimes were evident in the data. Olivier and Meyer [14] proved that hysteresis has no effect on the transitional flow regime, thus there was no need for additional measurements for increasing Reynolds numbers. The experimental data for the diabatic friction factor, as calculated with Equation 2.3, was plotted as a function of the Reynolds number in Figure 4.1. Also plotted in the laminar flow regime is the Poiseuille equation [19] and in the turbulent flow regime the Blasius equation [20]. The experimental results of Tam *et al.* [9] and Meyer *et al.* [15] are also shown.

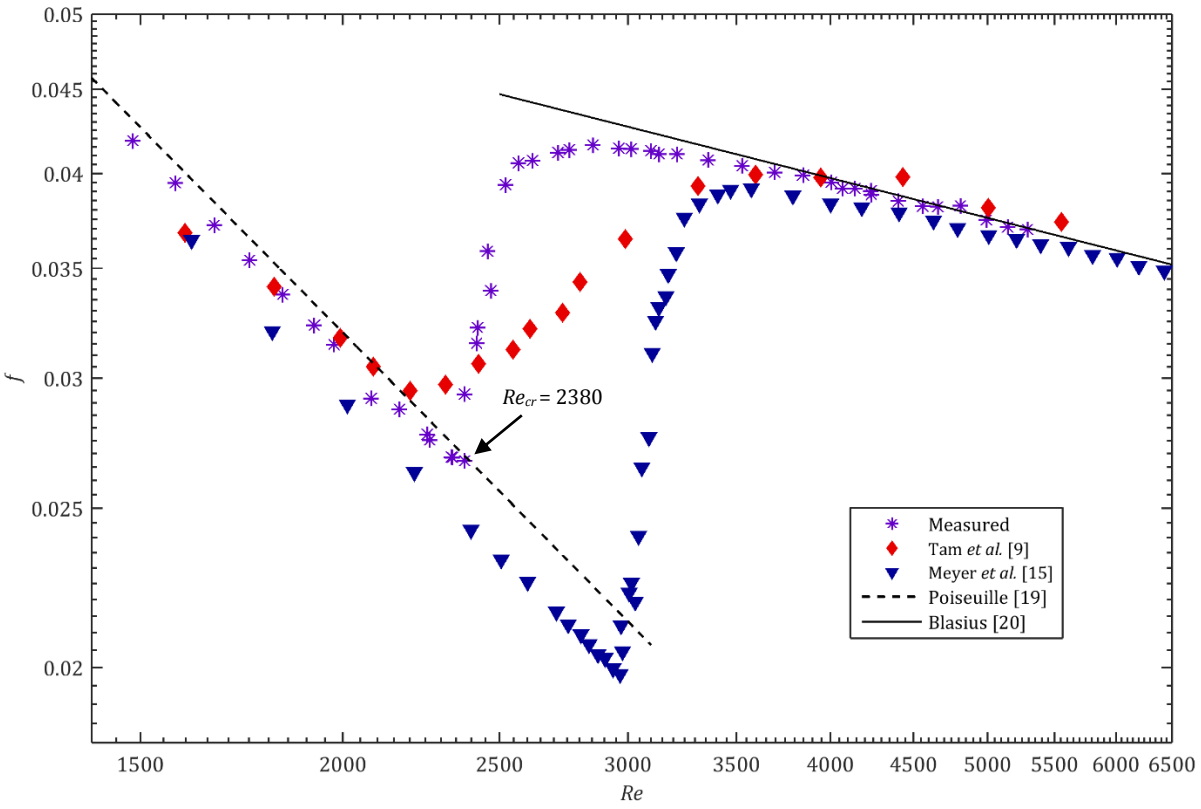

Figure 4.1: Friction factor as a function of Reynolds number for fully developed flow in a smooth tube with a constant heat flux boundary condition of 3 kW/m².

From Figure 4.1 it follows that the friction factor decreases linearly from a Reynolds number of 1 500 up to 2 380, indicating that the flow is in the laminar regime. At a critical Reynolds

number of 2 380 the friction factors increased significantly, indicating the start of transition. The data shows transition to last up to a Reynolds number of 3 090 where the turbulent flow regime starts.

The data showed the laminar friction factors to follow the gradient of the Poiseuille equation, with all the data points shifted slightly lower. This agreed with the findings of Tam *et al.* [9] and Meyer *et al.* [15] who showed that an increase in heat flux tends to decrease the friction factors in the laminar flow regime. The results of both these studies were plotted in Figure 4.1 for comparison to the current data. Both these studies used higher heat fluxes than the current study. Tam *et al.* [9] stated a heat flux in the range of 4.3 to 8.9 kW/m^2 was used, while Meyer *et al.* [15] used a value of 13 kW/m^2.

In the laminar flow regime (1 500 < Re < 2 300) the data showed an average difference of 2.7% and a maximum difference of 5% (at a Reynolds number of 2 080) when compared to the Poiseuille equation. In the turbulent flow regime the measured data showed an average and maximum difference of 0.7% and 2% (at a Reynolds number of 3 215) when compared to the Blasius equation. Most of the literature discussed in Chapter 2 found that heating tends to affect the laminar and early transitional flow regimes, which was the case in this study as well.

The modified Blasius equation [23] was considered, however, the viscosity ratio proved to be very close to unity because of the low heat flux used in this study. The Filonenko equation was also considered, however, according to Fang *et al.* [21] the Blasius equation would be more accurate in the Reynolds number range of this study (as discussed in Section 2.2.2).

When comparing the current experimental data to that of Meyer *et al.* [15], a significant difference could be seen in the laminar flow regime. However, this was to be expected as a much higher heat flux was used and the flow was not fully developed; while in this study the flow was fully developed. These experimental differences would tend to be most influential in the laminar and early transitional flow regimes, where secondary flow has a greater effect on the friction factors. Previous studies have proven that heating tends to delay the start of transition, which was also the case in this study when comparing the current results to that of Meyer *et al.* [15]. The start of transition correlated well to the findings of Tam *et al.* [9]. This could be because Tam *et al.* [9] used a heat flux closer to the current study than was used by Meyer *et al.* [15].

In the turbulent flow regime the results of the current study agreed with the findings of Tam *et al.* [9] and Meyer *et al.* [15].

In general, it can be concluded that the friction factor results as a function of Reynolds number compared very well with literature in the laminar and turbulent flow regimes. In the transitional flow regime the onset of transition occurred at a Reynolds number of 2 380. This compared very well with a large body of literature [2, 3, 18, 30]. The general trend of results in the transitional flow regime also compared well to that of two recent experimental studies [9, 15]. However, exact comparisons were not possible as the boundary values were not the same.

Furthermore, it can also be concluded that the validation results proved the accuracy of the friction factor results produced by the experimental set-up that was designed and constructed, the data reduction methodology, and experimental procedure that was implemented. Also that friction factor measurements can be produced in all three flow regimes of laminar, transitional and turbulent flow. This provided confidence that the original results produced in the following chapter, would be accurate.

4.3. SUMMARY AND CONCLUSIONS

In this chapter the experimental set-up, data acquisition system, data reduction method and experimental procedure were validated. A Single-tube with a constant heat flux boundary condition was tested for validation purposes. Pressure drop measurements, at different mass flow rates, were taken at the end of a long tube where the flow was fully developed. The mass flow rates were selected to ensure that a wide range of Reynolds numbers were covered over the laminar, transitional, and turbulent flow regimes. From the pressure drop and mass flow measurements the friction factors and Reynolds numbers were determined and the results were compared to literature. It was found that the results compared very well to literature in the laminar and turbulent flow regimes and the onset of transition also compared very well with literature and was found to occur at a critical Reynolds number of 2 380. After the onset of transition the general trend of the transition curve also corresponded well.

5. RESULTS

5.1. INTRODUCTION

This chapter is the most important of the study since its purpose is to present the pressure drop data for the triple-tube test section during diabatic fully-developed flow conditions. As stated in Chapter 3, three equally spaced tubes with a square-edged inlet condition were considered. In Chapter 4 the experimental set-up and testing procedure was validated and should serve as relative proof that the results presented in this chapter are accurate and correct. This chapter produces the results aligned to the purpose of this study as stated in Chapter 1. The conditions of the Single-tube investigation were repeated for each of the three tubes to find the effect of the adjacent tubes on the friction factor. The friction factor results were compared to the Single-tube case and some of the literature discussed in Chapter 2. The diabatic friction factors were presented as a function of Reynolds number and were discussed in three parts focussing on the laminar, turbulent and transitional flow regimes respectively. The raw and processed data can be found on the data repository CD and will be available from the supervisor only, after the oral examination of this dissertation.

5.2. SCOPE AND SUMMARY OF EXPERIMENTS

For clarification, the purpose of the experiments and the critical details are summarised in this section. The single-tube test section was used as the reference tube to validate the experimental set-up against previous studies (Chapter 4). With the triple-tube set-up, three tubes were spaced horizontally in-line by a pitch distance of 1.4 times the outer diameter, or 8.4 mm.

Each tube of the triple-tube test section was exactly the same as the tube of the single-tube test section. Stainless steel tubes were used with an inner diameter of 3.97 mm. The tubes were heated by direct current, each from its own power supplies; this ensured a constant heat flux of 3 kW/m^2 at the wall of each tube. The tubes were insulated from the environment to ensure minimal heat loss. The flow rate was measured using coriolis mass flow meters, one for each tube. The pressure drops were measured in the region of fully-developed flow using pressure transducers with three variable diaphragms to ensure the highest possible accuracy. The inlet temperature to the tubes was measured by a PT100 thermocouple probe mounted inside the calming section. The outlet bulk fluid temperature was measured for each tube by adding a mixer containing a PT100 thermocouple to the outlet of each tube.

Table 5.1: Experimental test matrix for the single-tube and triple-tube test sectionS.

		Number of measurements taken per tube				
Test-section	Reynolds number range	Flow rate	Pressure drop	Inlet temperature	Outlet temperature	Wall temperature
Single	1 472 - 2 444	15	15	15	15	585
Single	2 250 - 4 215	23	23	23	23	897
Single	4 049 - 5 268	9	9	9	9	351
Triple	1 054 - 2 49	15	15	15	15	585
Triple	2 304 - 4 439	25	25	25	25	975
Triple	4 070 - 6 242	10	10	10	10	390
	Total:	**97**	**97**	**97**	**97**	**3783**

The experiments that were conducted on the triple-tube and the single-tube test sections are summarised in Table 5.1. The test sections were set up to record pressure drop, mass flow rate, wall temperature, inlet fluid temperature and outlet fluid temperature values for each tube. The table shows that, for the single-tube test section, a total of 47 experiments were conducted. The experiments were split into three Reynolds number ranges corresponding to the range of each pressure transducer diaphragms used to take pressure drop measurements. In the case of the

triple-tube test section, 50 experiments were conducted. As was the case with the single-tube test section, three different pressure transducer diaphragms were used to ensure better accuracy, thus the experiments were split into three ranges.

5.3. DIABATIC FRICTION FACTOR

The friction factors are plotted as a function of Reynolds number in Figure 5.1 for the Single-tube and each tube of the triple-tube test section. The equations of Poiseuille and Blasius were also plotted for reference purposes. In this figure Tubes 1, 2 and 3 represent the left, centre and right tubes when facing the flow direction respectively, as identified in Figure 3.1. The Single-tube refers to the results taken from the single-tube test section as presented in Chapter 4.

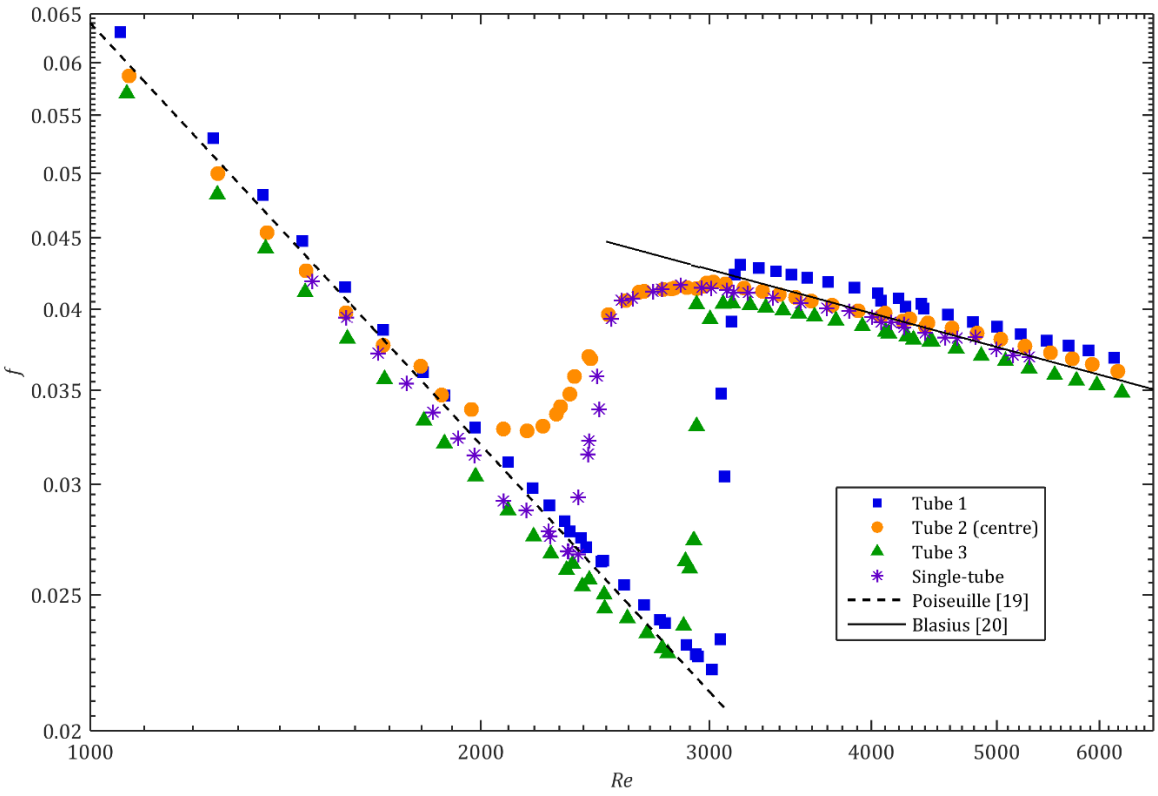

Figure 5.1: Diabatic friction factors as a function of Reynolds number for the Single-tube and each tube of the triple-tube test section with a heat flux of 3 kW/m² applied to each tube.

The results plotted in Figure 5.1 will be discussed in three parts, laminar, turbulent and transitional. In each part, the friction factor results are plotted in the Reynolds number range of interest to that section.

5.3.1. LAMINAR RESULTS

The laminar friction factors are plotted as a function of Reynolds number in Figure 5.2 for the Single-tube and each tube of the triple-tube test section. The equations of Poiseuille (laminar flow) and Blasius (turbulent) are also shown. Although the Reynolds number range of Figure 5.2 is from 1 000 to 3 500, for discussion purposes, the laminar results are only deliberated in this section for the Reynolds number range of 1 000 to 1 700.

The laminar friction factors for the triple-tube test section (that included Tubes 1, 2, and 3), corresponded well to the Poiseuille equation. The average difference between all three the triple-tube friction factors and the Poiseuille equation was 3.6%. The maximum difference was between Tube 3 and the Poiseuille equation which was 11.4% at a Reynolds number of 1 050.

The Centre-tube of the triple test section also compares well to the Single-tube experiments that were conducted for verification purposes (Chapter 4). The average error was less than 2% and the maximum error was 3%, which occurred at a Reynolds number of 1 750.

It is challenging to identify the reasons for the minor differences in the laminar friction factor values, as the differences in the laminar friction factors are in the same order of magnitude as their uncertainties. However, possible reasons were most probably combinations of the following: minor differences in the tube geometries (lengths and inner diameters), mixer geometries, flow meters, spacing between pressure taps, and installation of pressure tap holes.

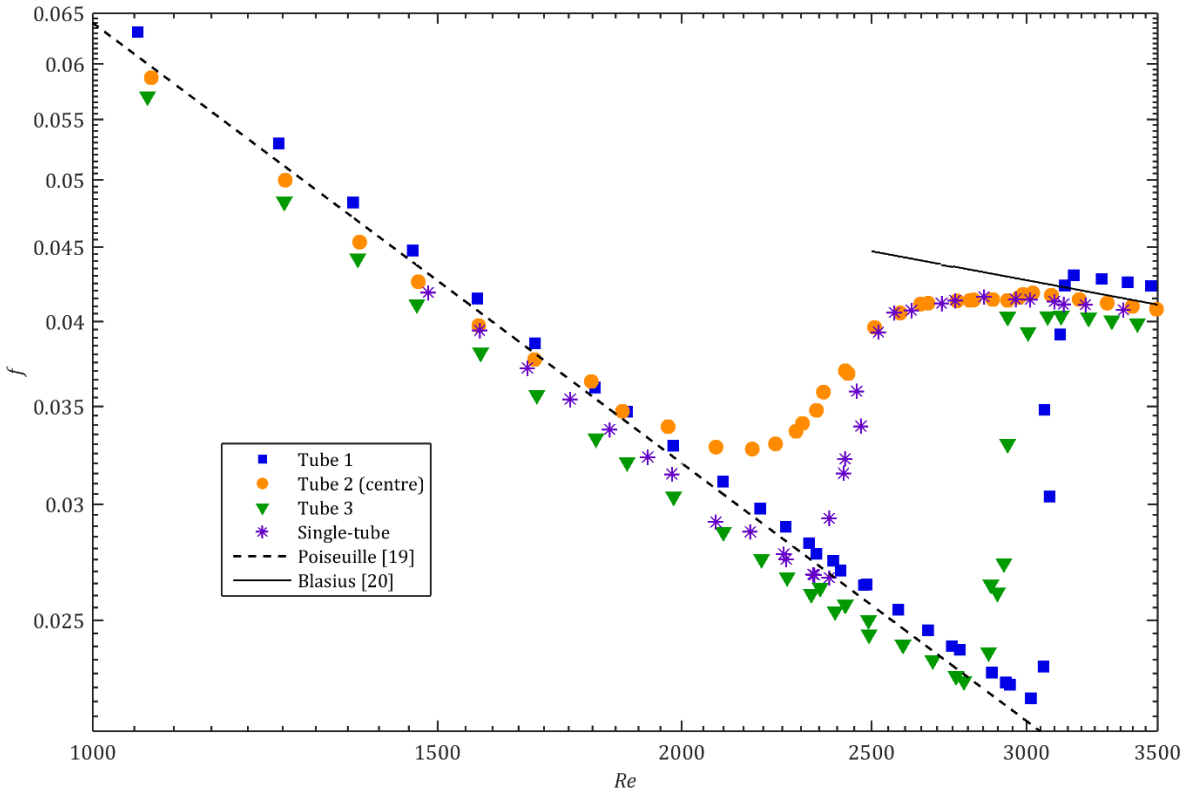

Figure 5.2: Diabatic friction factors as a function of Reynolds number for the Single-tube and each tube of the triple-tube test section with a heat flux of 3 kW/m² applied to each tube zoomed-in predominantly on the laminar flow regime.

The results from Figure 5.2 suggested that, in the laminar flow regime, inlet effects had no influence on the diabatic friction factors (in this case the inlet effects of adjacent tubes). This conclusion was also made by Ghajar and co-workers [9, 10] and Meyer and co-workers [4, 13-15].

5.3.2. TURBULENT RESULTS

The turbulent friction factors are plotted as a function of Reynolds number in Figure 5.3 for the Single-tube and each tube of the triple-tube test section. The Blasius equation is also plotted for comparison purposes. The Reynolds number selected for discussion purposes in the turbulent flow regime was between 3 500 and 6 500.

The friction factors for the triple-tube test section (that included Tubes 1, 2, and 3), correspond well to the Blasius equation. The average difference between all three the triple-tube friction factors and the Blasius equation was 2.3%. The maximum difference was with Tube 1, and the difference was 3.8%, at a Reynolds number of 4 370.

The Centre-tube of the triple test section also compared well to the Single-tube experiments that were conducted (Chapter 4) in the turbulent flow regime. The average difference was 1.3% and the maximum difference was 2%, which occurred at a Reynolds number of 4 830.

The diabatic friction factors in the turbulent flow regime were similar for all three tubes of the triple-tube test section. The Centre-tube followed the trend of the Single-tube closely, as was the case in the laminar flow regime. Tube 1 showed slightly higher friction factor values than Tube 3 in the turbulent flow regime. The difference in the friction factors of Tube 1 and Tube 3 (average of 5.8%) were slightly higher than the uncertainty (3%). As stated earlier, the slight differences between the friction factor values of the three tubes could be due to minor physical differences in the tubes, the mixers or the flow meters.

However, in general the results from Figure 5.3 confirmed that, in the turbulent flow regime, inlet effects had no influence on the diabatic friction factors. This agreed with the conclusions made by Ghajar and co-workers [9, 10] and Meyer and co-workers [4, 13-15].

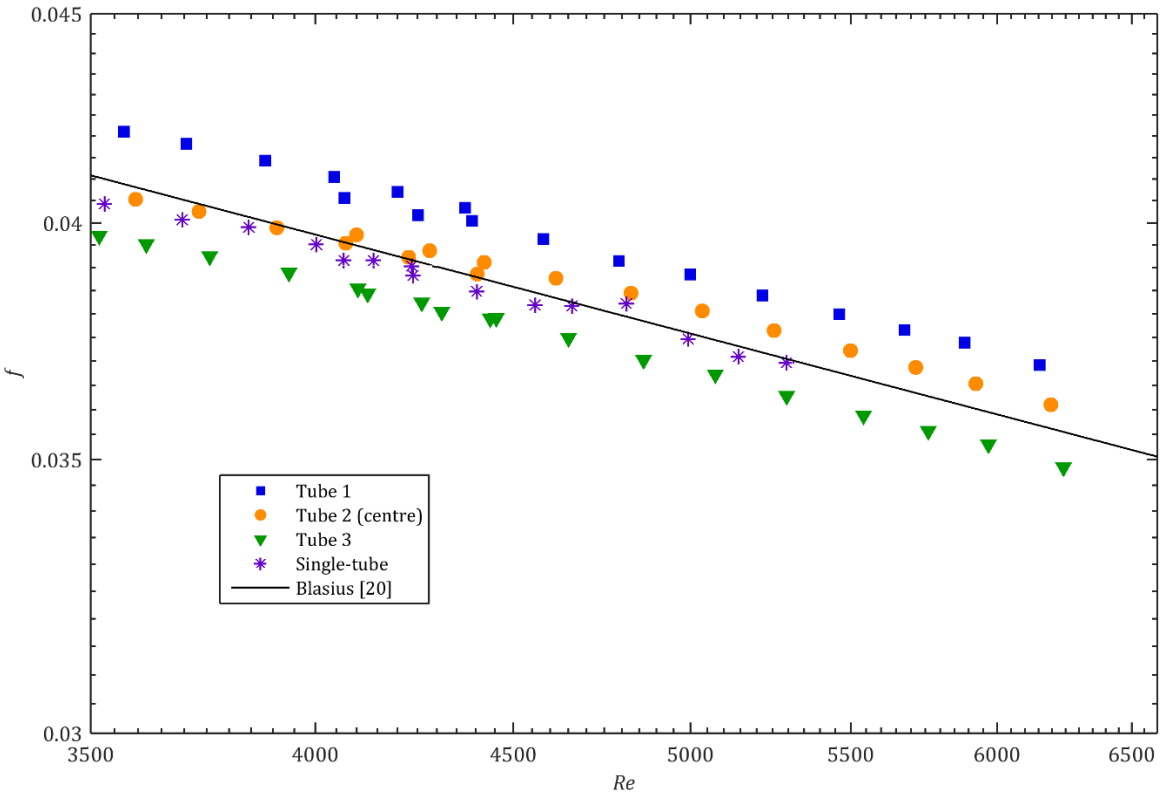

Figure 5.3: Diabatic friction factors as a function of Reynolds number for the Single-tube and each tube of the triple-tube test section with a heat flux of 3 kW/m² applied to each tube zoomed-in predominantly on the turbulent flow regime.

5.3.3. TRANSITIONAL RESULTS

The mainly transitional data are plotted as a function of Reynolds number in Figure 5.4 for the Single-tube and each tube of the triple-tube test section. The equations of Poiseuille (laminar flow) and Blasius (turbulent) are also shown. For discussion purposes, the transitional results will be focused in the Reynolds number range of 1 700 to 3 800.

For all three tubes of the triple-tube test section the transition from laminar to turbulent flow is shown in Figure 5.4. The diabatic friction factors followed a linearly decreasing pattern in both the laminar and turbulent flow regimes, but a clear increase in the transitional flow regime. A noticeable difference was evident in the transition of the Centre-tube (Tube 2) compared to the

adjacent tubes (Tubes 1 and 3). The Centre-tube showed an initial increase in its friction factor at a Reynolds number of 1 700 (Figure 5.4). The transition point was identified at a critical Reynolds number of 1 970. At this point the friction factors started to increase significantly. The transition of the Single-tube was at a higher Reynolds number of 2 380. Thus, the transition point of the centre tube was 17%, earlier than that of the Single-tube.

The end of transition for both the Centre-tube of the triple-test section and the single-tube test section were found to be at a Reynolds number of 3 050. This point was identified as the point where the gradient of the friction factor curve coincided with the gradient of the Blasius equation. The gradient of transition, between the points where transition started and ended, of the Single-tube was much higher than that of the Centre-tube. The transition curve for the Centre-tube showed a lower gradient, leading to a longer transition period. Transition in the case of the Single-tube showed a much steeper gradient than that of the Centre-tube, leading to an abrupt transition.

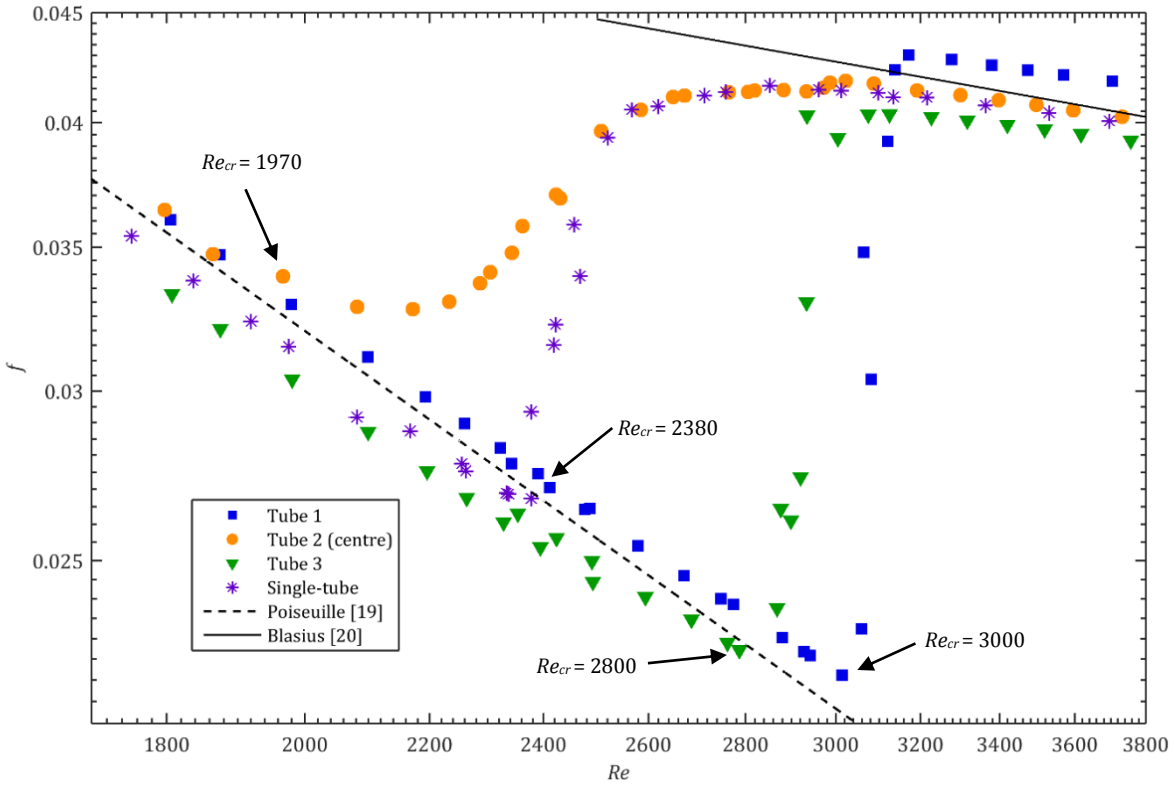

Figure 5.4: Diabatic friction factors as a function of Reynolds number for the Single-tube and each tube of the triple-tube test section with a heat flux of 3 kW/m² applied to each tube zoomed-in predominantly on the transitional flow regime.

Tube 1 and 3 showed significantly dissimilar behaviour to that of the Centre-tube and to that of the Single-tube, when comparing the start of transition. Tube 1 entered transition at a Reynolds number of 3 000, 26% later than the Single-tube and 58% later than the Centre-tube. The same trend was seen in Tube 3, entering transition at a Reynolds number of 2 800, 18% and 42% later than the Single-tube and Centre-tube respectively. The transition for both tubes was short and steep (in terms of friction factors), with transition ending at Reynolds number of 3 150 and 3 080 for tubes 1 and 3 respectively. Thus, when comparing the adjacent tubes to the Single-tube and Centre-tube, the friction factors showed the start of transition to be delayed significantly, but the end of transition to be similar.

The start and end of transition for each tube of the triple-tube test section, as well as for the Single-tube test section are summarised in Table 5.2.

Table 5.2: The start and end of transition, in terms of Reynolds numbers, for the Single-tube and each tube of the triple-tube test section during diabatic conditions.

	Start of transition, Re_{cr}	End of transition
Single-tube	2 380	3 050
Tube 1	3 000	3 150
Tube 2 (Centre)	1 970	3 050
Tube 3	2 800	3 080

From the values of Table 5.1 the conclusion could be drawn that adjacent tubes only have a significant effect on the start of transition in diabatic conditions, with the start of transition being provoked by the adjacent tubes. Thus, the inlet effects caused by adjacent tubes affected the start of transition, but not the end of transition, which agreed with the findings of Ghajar and co-workers [9, 10], as well as Meyer and co-workers [4, 13-15].

The diabatic friction factor results showed that the Centre-tube enters transition much earlier than the outer tubes. From Figure 5.1 it follows that, in the Reynolds number range of 2 300 to 2 800, the Centre-tube had considerably higher friction factor values than the two outer tubes. Therefor the Centre-tube, having a higher flow resistance, would receive less flow than the outer tubes in this flow range.

The extent of flow maldistribution was studied by investigating the mass flow rates in three Reynolds number ranges (Table 5.3). The first and last Reynolds number range of Table 5.3 correspond to fully laminar and fully turbulent conditions in all three tubes respectively, while the middle range corresponds to the case when the flow regimes are in the transitional phase. The average mass flow rate of the outer tubes was compared to the mass flow rate in the Centre-tube and the percentage difference was calculated. Table 5.3 summarises the findings:

Table 5.3: The average flow rate of the outer tubes compared to the flow rate of the inner tube presented as a percentage difference for three Reynolds number ranges.

Reynolds number range	Average Centre-tube difference
1 050 – 1 970	0.6% (higher)
1 970 – 3 150	2.8% (lower)
3 150 – 6 240	0.1% (lower)

The results of Table 5.3 show maldistribution in the region where the Centre-tube had started transition while the outer tubes were still in laminar flow.

5.4. SUMMARY AND CONCLUSIONS

In this chapter the experimental results were presented for the triple-tube test section under diabatic conditions. The friction factors were plotted as a function of Reynolds number and the results of each tube were analysed and discussed. Comparisons were made to the friction factor results of the single-tube test section under the same conditions.

The laminar results showed little difference between the friction factors of the three tubes, and similarities could clearly be seen to the friction factors of the Single-tube. The laminar friction factors correlated well to the Poiseuille equation for all three tubes with an average difference of only 3.6%.

The turbulent results also showed little difference between the friction factors of the three tubes and similarities to the results of the Single-tube tests. The turbulent friction factors correlated well to the Blasius equation for all three tubes with an average difference of 2.3%.

The diabatic friction factor results showed the start of transition to be significantly affected by adjacent tubes. The Centre-tube (Tube 2) of the triple-tube test section entered transition earlier than the adjacent tubes (Tubes 1 and 3), and also earlier than the tube from the single-tube test section. The left and right tubes both saw a delay in transition when compared to the Single-tube case. However, all three tubes of the triple-tube test section saw transition ending at a similar Reynolds number, leading to the conclusion that adjacent tubes tend to affect only the start of transition.

In general it can thus be concluded that neighbouring tubes will have a significant effect on the friction factors of tubes if they are operated in the transitional flow regime, especially in the region close to the onset of transition.

6. SUMMARY, CONCLUSIONS AND RECOMMENDATIONS

6.1 SUMMARY

With our world's ever growing population, energy generation has become one of the biggest challenges for modern engineers. Most power stations convert thermal energy into usable electricity with the help of highly specialised heat exchangers. Heat exchangers are not unique to the energy generation sector, but can be seen throughout daily life in our cars, fridges and air-conditioning systems. Efficiency is a key factor in the design of any heat exchanger and many design guides are available. Most of these design guides recommend staying away from the transitional flow regime, since flow in this regime can be unpredictable. However, modern heat exchangers are often forced to work in the transitional flow regime, due to design constraints, climate considerations, scaling and corrosion. Furthermore, when the flow is not perfectly distributed through all the tubes of a heat exchanger (such as a shell-and-tube heat exchanger), some tubes might operate in the transitional flow regime.

Tube flow has been extensively investigated since the 19th century. The flow conditions were categorised as laminar flow, turbulent flow and a transitional stage where the flow acts laminar at times and turbulent at other times, now known as the transitional flow regime. The laminar and turbulent flow regimes are well understood, with good correlations available in literature to predict the flow characteristics. The transitional regime, however, is less well understood. Most of the research into the transitional flow regime, for horizontal circular tubes, investigated inlet effects with and without heat transfer. Some studies have also been done on enhanced tubes, nanofluids, micro-channels and developing flow. However, all of these studies focussed only on a single tube. Knowing that heat exchangers make use of a bundle of tubes, the problem statement of this study was identified. With this gap in literature identified, the purpose of this study was to investigate the effect of adjacent tubes on the transitional flow regime.

To address the aim of this study, an experimental set-up was designed and built specifically for the current study. Two test sections were built, a single-tube test section and a triple-tube test section which hosted three tubes horizontally spaced by a pitch distance of 1.4 outside diameters. Each tube had an inside diameter of 3.97 mm and a full length of 6 m. The pressure drop could be measured over the fully-developed section (last 1.97 of tube) of each tube and wall temperature measurements could be taken over the entire length. A calming section was used at the inlet of each test section and mixers were placed at the outlet of each tube. The calming section and each mixer hosted a thermocouple to measure the inlet and outlet average fluid temperature. Each tube was connected to its own mass flow meter and a manifold was installed at the outlet of the triple-tube test section to ensure each tube had the same outlet condition. An uncertainty analysis was conducted to show the relevant uncertainties in the measurements and results. The outcome showed that the highest uncertainties resided in the transitional flow regime due to the instability of the flow rate. However, the uncertainties of the Reynolds number and friction factor remained below 4% and 8.3% in all cases respectively.

6.2. CONCLUSIONS

The single-tube test section was investigated first since it could be compared to recent studies with similar conditions. A heat flux of 3 kW/m^2 was used and the flow was decreased from a Reynolds number of 5 300 down to 1 500. The diabatic friction factors were compared to the Poiseuille and Blasius equations, as well as recent similar studies. The friction factors correlated well to the equations of Poiseuille and Blasius in the laminar and turbulent flow regimes respectively. The laminar friction factors showed a slight downward shift to the Poiseuille equation, which agreed with recent studies. When comparing the data to other experimental studies agreement could be seen, especially in the turbulent flow regime.

The triple-tube test section was tested under the same conditions as the single-tube case. The friction factors were plotted as a function of Reynolds number for each tube. In the laminar flow regime the friction factor results showed little difference between the three tubes, and similarities could clearly be seen to the Single-tube results. The results showed the start of transition to be significantly affected by adjacent tubes during diabatic conditions. The middle tube entered transition much earlier than the left and right tube and also earlier than the Single-tube. The left and right tubes both saw a delay in transition when compared to the Single-tube case. The results showed the end of transition to be unaffected by the adjacent tubes, since all three tubes entered the turbulent flow regime at similar Reynolds numbers to that of the Single-tube case. The turbulent friction factors were similar in all three tubes and also analogous to the results of the Single-tube case.

The results of this study could also give some insight into flow maldistribution through tube bundles. The friction factor results showed the Centre-tube to enter transition much earlier than the outer tubes. This led to the friction factors of the Centre-tube being significantly higher than those of the outer tubes in the Reynolds number range of 1 970 to 3 150. The flow rates through the outer tubes were compared to that of the inner tube, and average difference of 2.8% (lower) was found in this Reynolds number range. Maldistribution proved to be negligible when all three tubes were in the laminar or turbulent flow regimes.

6.3. RECOMMENDATIONS

The following recommendations are made for future work:

- Different tube pitches could be investigated.
- A 3-dimensional study could be done, with tubes spaced vertically and horizontally. Different tube layouts can then be investigated as well.
- Different heat fluxes can be investigated.
- Enhanced tubes could be used in place of smooth tubes.

7. REFERENCE LIST

[1] P. Breeze, Power Generation Technologies, Elsevier Science, 2005.
[2] Y.A. Çengel, A. Ghajar, Heat and Mass Transfer (A Practical Approach, SI Version), in, McGraw-Hill Education, 2011.
[3] J.H. Lienhard, A heat transfer textbook, Courier Corporation, 2013.
[4] J.P. Meyer, Heat transfer in tubes in the transitional flow regime, in: Proceedings of the 15th International Heat Transfer Conference, Kyoto, paper KN03, 2014, pp. 11-15.
[5] M.I. Kim, Y. Lee, B.W. Kim, D.H. Lee, W.S. Song, CFD modeling of shell-and-tube heat exchanger header for uniform distribution among tubes, Korean Journal of Chemical Engineering, 26(2) (2009) 359-363.
[6] S. Lalot, P. Florent, S. Lang, A. Bergles, Flow maldistribution in heat exchangers, Applied thermal engineering, 19(8) (1999) 847-863.
[7] K. Wang, X.-C. Tu, C.-H. Bae, H.-B. Kim, Optimal design of porous baffle to improve the flow distribution in the tube-side inlet of a shell and tube heat exchanger, International Journal of Heat and Mass Transfer, 80 (2015) 865-872.
[8] A.J. Ghajar, K.F. Madon, Pressure drop measurements in the transition region for a circular tube with three different inlet configurations, Experimental thermal and fluid science, 5(1) (1992) 129-135.
[9] H.K. Tam, L.M. Tam, A.J. Ghajar, Effect of inlet geometries and heating on the entrance and fully-developed friction factors in the laminar and transition regions of a horizontal tube, Experimental thermal and fluid science, 44 (2013) 680-696.
[10] L.-M. Tam, A.J. Ghajar, Effect of inlet geometry and heating on the fully developed friction factor in the transition region of a horizontal tube, Experimental thermal and fluid science, 15(1) (1997) 52-64.
[11] J.P. Meyer, J. Olivier, Transitional flow inside enhanced tubes for fully developed and developing flow with different types of inlet disturbances: Part I–Adiabatic pressure drops, International Journal of Heat and Mass Transfer, 54(7) (2011) 1587-1597.
[12] J.P. Meyer, J. Olivier, Transitional flow inside enhanced tubes for fully developed and developing flow with different types of inlet disturbances: Part II–heat transfer, International Journal of Heat and Mass Transfer, 54(7) (2011) 1598-1607.
[13] J.P. Meyer, J.A. Olivier, Heat transfer and pressure drop characteristics of smooth horizontal tubes in the transitional flow regime, Heat Transfer Engineering, 35(14-15) (2014) 1246-1253.
[14] J. Olivier, J.P. Meyer, Single-phase heat transfer and pressure drop of the cooling of water inside smooth tubes for transitional flow with different inlet geometries (RP-1280), HVAC&R Research, 16(4) (2010) 471-496.
[15] J.P. Meyer, T. McKrell, K. Grote, The influence of multi-walled carbon nanotubes on single-phase heat transfer and pressure drop characteristics in the transitional flow regime of smooth tubes, International Journal of Heat and Mass Transfer, 58(1) (2013) 597-609.
[16] J. Dirker, J.P. Meyer, D.V. Garach, Inlet flow effects in micro-channels in the laminar and transitional regimes on single-phase heat transfer coefficients and friction factors, International Journal of Heat and Mass Transfer, 77 (2014) 612-626.
[17] M. Everts, Heat transfer and pressure drop of developing flow in smooth tubes in the transitional flow regime, University of Pretoria, 2014.
[18] F.M. White, Fluid mechanics, McGraw-Hill, New York, (2003).
[19] J.L. Poiseuille, Recherches expérimentales sur le mouvement des liquides dans les tubes de très-petits diamètres, Imprimerie Royale, 1844.
[20] H. Blasius, Das Ähnlichkeitsgesetz bei Reibungsvorgängen in Flüssigkeiten, Springer, 1913.
[21] X. Fang, Y. Xu, Z. Zhou, New correlations of single-phase friction factor for turbulent pipe flow and evaluation of existing single-phase friction factor correlations, Nuclear Engineering and Design, 241(3) (2011) 897-902.

[22] M. Danish, S. Kumar, S. Kumar, Approximate explicit analytical expressions of friction factor for flow of Bingham fluids in smooth pipes using Adomian decomposition method, Communications in Nonlinear Science and Numerical Simulation, 16(1) (2011) 239-251.
[23] R. Allen, E. Eckert, Friction and heat-transfer measurements to turbulent pipe flow of water (Pr= 7 and 8) at uniform wall heat flux, Journal of Heat Transfer, 86(3) (1964) 301-310.
[24] B.S. Petukhov, A. Polyakov, B.E. Launder, Heat transfer in turbulent mixed convection, (1988).
[25] T.H. Chilton, A.P. Colburn, Mass transfer (absorption) coefficients prediction from data on heat transfer and fluid friction, Industrial & engineering chemistry, 26(11) (1934) 1183-1187.
[26] O. Reynolds, An experimental investigation of the circumstances which determine whether the motion of water shall be direct or sinuous, and of the law of resistance in parallel channels, Proceedings of the royal society of London, 35(224-226) (1883) 84-99.
[27] L.F. Moody, Friction factors for pipe flow, Trans. Asme, 66(8) (1944) 671-684.
[28] H.K. Tam, L.M. Tam, A.J. Ghajar, S.C. Tam, T. Zhang, Experimental investigation of heat transfer, friction factor, and optimal fin geometries for the internally microfin tubes in the transition and turbulent regions, Journal of enhanced heat transfer, 19(5) (2012).
[29] S.o.t.T.E.M. Association, Tubular Exchanger Manufacturers Association, Inc., Tarrytown, New York, (2007).
[30] R. Mukherjee, Effectively design shell-and-tube heat exchangers, Chemical Engineering Progress, 94(2) (1998) 21-37.
[31] A.P. Fraas, Heat exchanger design, John Wiley & Sons, 1989.
[32] A. Bakker, R.D. LaRoche, E.M. Marshall, Laminar flow in static mixers with helical elements, The online CFM Book, http://www. bakker. org/cfm, (1998).
[33] R. Rayle, Influence of orifice geometry on static pressure measurements, American Society of Mechanical Engineers, 1959.
[34] C. Popiel, J. Wojtkowiak, Simple formulas for thermophysical properties of liquid water for heat transfer calculations (from 0 C to 150 C), Heat transfer engineering, 19(3) (1998) 87-101.
[35] P.F. Dunn, Measurement and data analysis for engineering and science, CRC press, 2014.

APPENDIX A: PHOTOS OF THE LABORATORY, EXPERIMENTAL SET-UP AND TEST SECTIONS

Figure A.1: Photo showing the experimental set-up and laboratory. The schematic of Figure 3.1 can be compared to the photo for a better understanding of the equipment shown here.

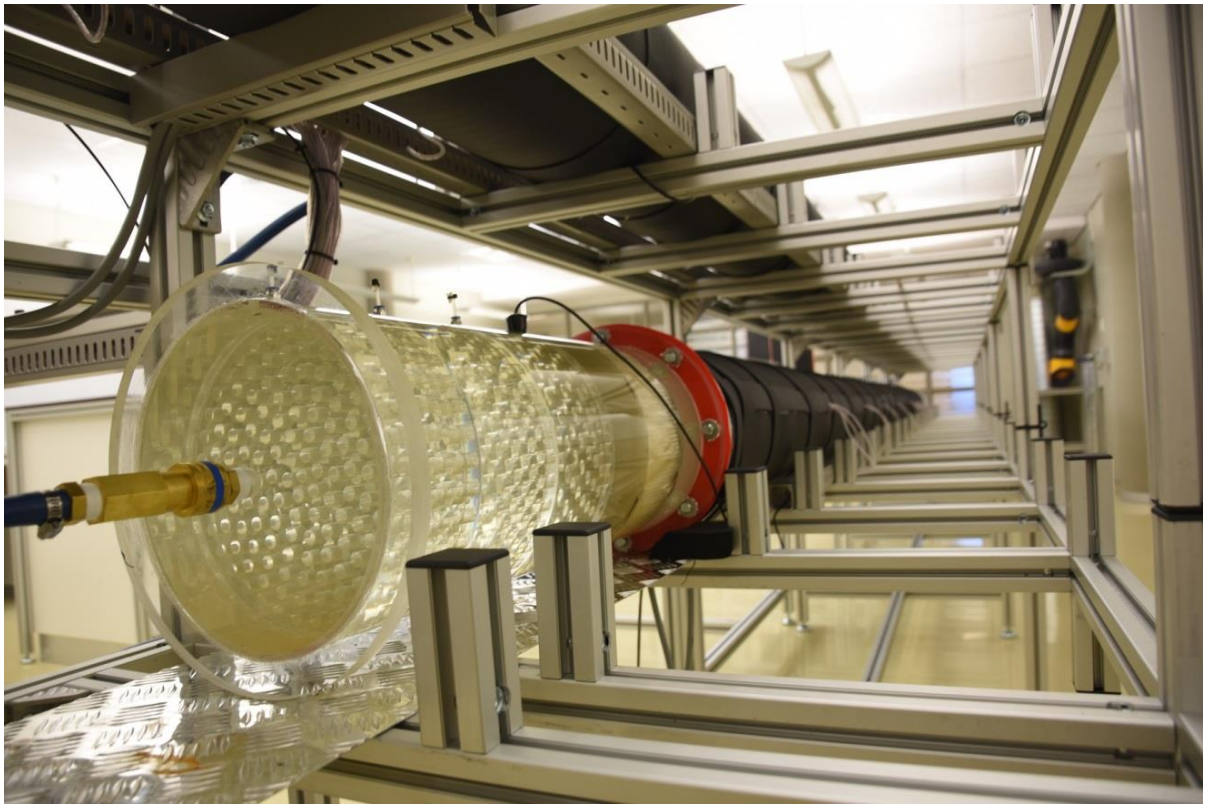

Figure A.2: Photo showing the calming section and start of the test section. The test section is surrounded by thermal insulation in this photo, however, the thermocouple wires can be seen protruding from the insulation along the length of the test section.

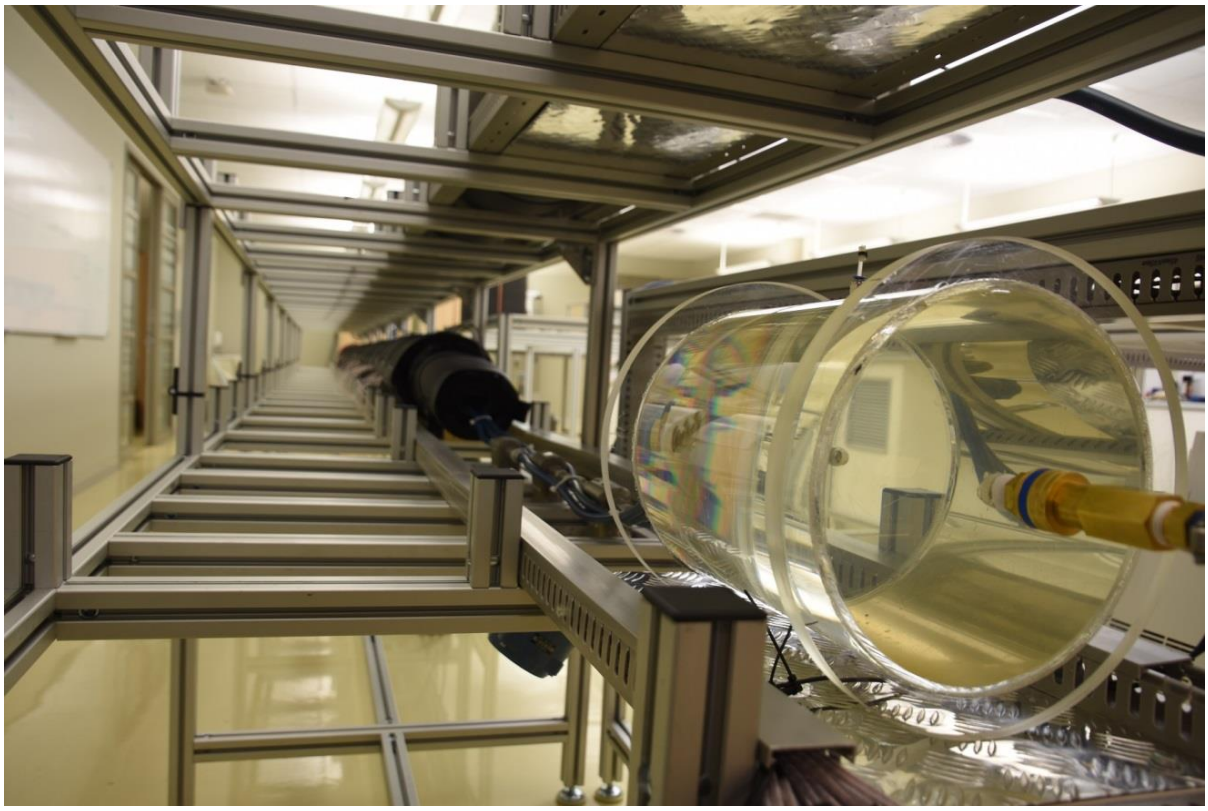

Figure A.3: Photo showing the end of the test section, coriolis mass flow meters and manifold. The mass flow meters can be seen in their staggered positions. The mixers cannot be seen as they are surrounded by insulating material.

Figure A.4: Photo showing the flow meter displays, power supplies, data acquisition system and computer.

Figure A.5: Photo showing the full length of the insulated test section (bottom shelf). The table in the centre of this photo is exactly the same as the table in Figure A.1, thus everything added to the table in Figure A.1 was done by the Author and 2 fellow students in the time frame of 8 months.